

# Nitridosilicates and Oxonitridosilicates: From Ceramic Materials to Structural and Functional Diversity

Martin Zeuner, Sandro Pagano, and Wolfgang Schnick\*

**Keywords:**  
ceramic materials · luminescence ·  
nitridosilicates ·  
solid-state structures

*In memory of Friedrich Liebau*



Angewandte  
Chemie

**S**ilicates are one of the most important classes of compounds on this planet, and more than 1000 silicates have been identified in the mineral kingdom. Additionally, several hundreds of artificial silicates have been synthesized. The substitution of oxygen by nitrogen leads to the structurally diverse and manifold class of nitridosilicates. Silicon nitride, one of the most important non-oxidic ceramic materials, is the binary parent compound of nitridosilicates, and it symbolizes the inherent material properties of these refractory compounds. However, prior to the last decades, a broad systematic investigation of nitridosilicates had not been accomplished. In the meantime, these and related compounds have reached a remarkable level of industrial application. This review illustrates recent progress in synthesis and structure–property relationships and also applications of nitridosilicates, oxonitridosilicates, and related SiAlONs.

## From the Contents

<b>1. Introduction</b>	7755
<b>2. Synthetic Approaches</b>	7756
<b>3. 1D Nitridosilicates</b>	7758
<b>4. 2D Nitridosilicates</b>	7759
<b>5. 3D Nitridosilicates</b>	7760
<b>6. Chemical Bonding in Nitridosilicates</b>	7766
<b>7. Material Properties</b>	7768
<b>8. Outlook</b>	7771

### 1. Introduction

With respect to occurrence, silicates dominate all other compound classes on this planet. This is due to the fact that silicon and oxygen are by far the most abundant chemical elements, accounting approximately for three quarters of the earth's mass with respect to both crust and mantle. Silicate minerals, such as enstatite, quartz, or plagioclase, are much more prevalent than most other minerals.<sup>[1,2]</sup> Silicate-based man-made accomplishments, such as pottery, glassware, porcelain, cement, and concrete, or modern micro- or mesoporous silicate materials, are symbols of the cultural, technical, and scientific development on this planet. Even the origin of life could possibly be traced back to a self-assembly of biomolecules on silicate surfaces.<sup>[3,4]</sup> Until the 1950s, silicate chemistry was more or less limited to variation of complex Si/O substructures and their dimensionality and the exchange of the electropositive counterions. Pursuing the idea of an oxometalate-analogous chemistry of nitridometalates, Juza et al. entered the field of nitridosilicates in 1953 by studying the quasi-binary system Li<sub>3</sub>N–Si<sub>3</sub>N<sub>4</sub>.<sup>[5]</sup> However, for several decades, nitrides have only been of minor scientific and technological relevance in comparison to the large and manifold world of oxides. Then, the growing technological impact of advanced non-oxidic materials boosted scientific interest in high-performance ceramics, such as silicon nitride (Si<sub>3</sub>N<sub>4</sub>) or aluminum nitride (AlN).<sup>[6–8]</sup> Partial substitution of Si by Al and N by O in Si<sub>3</sub>N<sub>4</sub> led to the discovery of so-called SiAlONs by Oyama and Jack in the early 1970s.<sup>[9,10]</sup> However, it was not before the late 1980s that a broad synthetic approach to the manifold world of nitridosilicates started to develop.<sup>[7]</sup> Typically, nitridosilicates do not occur naturally. This finding is a direct consequence of the high oxygen partial pressure and the omnipresence of water on our planet. Furthermore, most solid oxides are more stable than nitrides because chemical bonds to nitrogen are typically less stable than bonds to oxygen. Thus, in the presence of water, bonds to

nitrogen can undergo hydrolysis, unless a high degree of condensation within the nitride kinetically prevents this dissociation.<sup>[7]</sup> The only naturally occurring (oxo)nitridosilicate mineral is sinoite, Si<sub>2</sub>N<sub>2</sub>O, which however usually originates from meteorites.<sup>[11,12]</sup> The latter observation might be an indication of the existence of other planets or asteroids that are made up predominantly of nitridosilicates and/or oxonitridosilicates owing to the absence of oxygen and the presence of a higher nitrogen partial pressure.<sup>[2]</sup>

Creating synthetic nitridosilicates means much more than simply substituting O by N in classical (oxo)silicates, because introduction of nitrogen leads to significantly extended structural possibilities. Typically, oxosilicates and nitridosilicates are made up of more or less condensed [SiO<sub>4</sub>] and [SiN<sub>4</sub>] tetrahedra, respectively. However, unlike the structural situation of oxygen in classical (oxo)silicates, nitrogen exhibits more varied crosslinking patterns in nitridosilicates. While oxygen can only be terminally bound to Si (denoted as O<sup>[1]</sup>) or is simply bridging (O<sup>[2]</sup>), nitrogen occurs as N<sup>[1]</sup>, N<sup>[2]</sup>, N<sup>[3]</sup>, and even ammonium-type N<sup>[4]</sup>, connecting up to four neighboring Si tetrahedral centers.<sup>[13]</sup> Furthermore, in nitridosilicates, [SiN<sub>4</sub>] tetrahedra can share both common corners and common edges,<sup>[13]</sup> while oxosilicates nearly exclusively contain corner-sharing [SiO<sub>4</sub>] tetrahedra. The only exception from the rule reported to date is fibrous SiO<sub>2</sub>, whose existence has not yet been proven unequivocally.<sup>[14]</sup> Another important consequence of O/N substitution in silicates is the significantly extended range for the degree of condensation  $\kappa$ , that is, the molar ratio Si:(O,N). The lowest value  $\kappa = \frac{1}{4}$  corre-

[\*] Dr. M. Zeuner, Dr. S. Pagano, Prof. Dr. W. Schnick  
 Ludwig-Maximilians-Universität, Lehrstuhl für Anorganische Festkörperchemie, Department Chemie  
 Butenandtstrasse 5-13 (D), 81377 München (Germany)  
 Fax: (+49) 89-2180-77440  
 E-mail: wolfgang.schnick@uni-muenchen.de  
 Homepage: <http://www.cup.uni-muenchen.de/ac/schnick/>

sponds to non-condensed tetrahedral anions  $[\text{SiO}_4]^{4-}$  and  $[\text{SiN}_4]^{8-}$ , while the maximum value is reached in case of the binary species  $\text{SiO}_2$  ( $\kappa = \frac{1}{2}$ ) and  $\text{Si}_3\text{N}_4$  ( $\kappa = \frac{3}{4}$ ), respectively. In silicate chemistry, no higher  $\kappa$  values seem possible as they would lead to cationic silicate substructures that have never been observed.<sup>[1,2,7,13]</sup> Substitution of O by N in silicates can be accompanied additionally by substitution of Si by Al, leading to so-called SiAlONs (oxonitridoalumosilicates), which by analogy to silicates are typically made up of  $[\text{TX}_4]$  tetrahedra (T = Al, Si and X = O, N). From a systematic point of view, SiAlONs represent the superordinate class of compounds, and oxosilicates, nitridosilicates, oxonitridosilicates, and nitridoalumosilicates are subgroups thereof. Consequently, the manifold group of oxosilicates could be interpreted to form a subset of the even more varied class of SiAlONs.

Recently, Eu<sup>2+</sup>-doped nitridosilicates and oxonitridosilicates emerged as highly effective optical materials affording phosphor-converted light-emitting diodes (pc-LEDs) based on high-power primary blue GaN-based LEDs. These devices have the potential to entirely replace both incandescent and fluorescent lamps, with dramatic global energy-saving capability.<sup>[15]</sup>

As compared with oxosilicates, structures of nitridosilicates, oxonitridosilicates, and related SiAlONs can be even more complex and varied. Therefore, in this contribution the degree of condensation and the dimensionality of the (oxo)nitridosilicate substructures are employed as means to classify these compounds. The main emphasis of this review is on recent synthetic advances and an understanding of structure-property relations as well as applications of this fascinating class of materials.

## 2. Synthetic Approaches

The binary parent compound of nitridosilicates is silicon nitride ( $\text{Si}_3\text{N}_4$ ).<sup>[7]</sup> It has increasingly gained relevance for the development of ceramic materials for high-performance applications owing to excellent thermal, mechanical, and chemical stability combined with low density. Practical applications include substrates for semiconductors on the basis of  $\text{Si}_3\text{N}_4$  or high-temperature materials such as valve tappets, turbochargers, and other refractory materials.<sup>[7,16]</sup> Furthermore, doping with rare earth metals can even improve the mechanical properties of silicon nitride ceramics.<sup>[17–19]</sup>



*Wolfgang Schnick, born in 1957, studied chemistry in Hannover, where he received his doctorate under supervision of Martin Jansen in 1986. After a year as a postdoctoral fellow at the Max-Planck Institute for solid-state research in Stuttgart, he finished his habilitation in 1992 at the University of Bonn. In 1993 he was appointed as full professor at the University of Bayreuth. Since 1998 he has held the chair of inorganic solid-state chemistry at the University of Munich (LMU), where he currently is the head of the Department of Chemistry.*

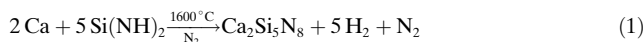
For a long time  $\text{Si}_3\text{N}_4$  had not been used as starting material for the synthesis of multinary nitrides. A varied chemistry, comparable to that of oxido borates, silicates, or phosphates, which derives by formal exchange of oxygen by nitrogen, had not been established until the late 1980s.<sup>[7,13]</sup> The most important reason for the lack of knowledge concerning multinary nitridosilicates was the high chemical and thermal stability of  $\text{Si}_3\text{N}_4$ . On one hand, this inertness is an important precondition for an application of this ceramic material in high-temperature and high-performance applications. On the other, its refractory properties seem to impede significantly its employment as a starting material in chemical syntheses.

### 2.1. High-Temperature Reactions

(Oxo)nitridosilicates can be synthesized by a broad spectrum of different approaches. For example,  $\text{MgSiN}_2$  was prepared by reaction of the binary nitrides,  $\text{MnSiN}_2$  from metallic Mn, and  $\text{RESi}_3\text{N}_5$  (RE = rare earth element) by nitriding two-phase alloys with composition  $\text{RESi}_3$ . Frequently, these classical reactions have been performed at elevated temperatures in the range of 1550–1750 °C; however, silicon nitride ( $\text{Si}_3\text{N}_4$ ) and moreover rare earth nitrides exhibit only low chemical reactivity<sup>[20]</sup> owing to low interdiffusion coefficients in solid-state reactions. Therefore, synthetic approaches leading to ternary and multinary (oxo)nitridosilicates had to be developed, abandoning the use of binary nitrides and treating the pure metals with silicon diimide ( $\text{Si}(\text{NH})_2$ ) instead. This approach proved to be successful for the synthesis of a variety of nitridosilicates.<sup>[13]</sup> Silicon diimide is an amorphous and still relatively undefined but reactive compound, which is converted into amorphous  $\text{Si}_3\text{N}_4$  at temperatures above 900 °C. It is synthesized by ammonolysis of  $\text{SiCl}_4$  and represents an important precursor for the technical production of  $\text{Si}_3\text{N}_4$  ceramics.<sup>[6]</sup> The reactions between a metal and  $\text{Si}(\text{NH})_2$  may be interpreted as the dissolution of an electropositive metal in the nitrido-analogous, polymeric “acid”  $\text{Si}(\text{NH})_2$ , accompanied by  $\text{H}_2$  evolution. Owing to an increase of the degree of condensation, ammonia may be formed as a side product, which dissociates into hydrogen and nitrogen at reaction temperatures above 1000 °C [Eq. (1)]. In several cases, the degree of condensation  $\kappa$  (that is, molar ratio Si:N) increases and highly condensed nitridosilicates (Si:N > 1:2) are formed.



*Martin Zeuner, born 1981 in Munich, studied chemistry at the University of Munich (LMU) and received his PhD in 2009 under the guidance of Wolfgang Schnick with a thesis on molecular precursor chemistry and solid-state synthesis of nitridosilicate phosphors for LED applications. Until recently, he led the LED research team in Schnick's group, and he has then accepted a position in the chemical industry.*



However, there are also indications that a nitridation process of the employed metals initially occurs, followed by reaction with silicon nitride, which has formed by thermal treatment of silicon diimide. Nevertheless, as two binary nitrides are formed *in situ*, both of them exhibit sufficient reactivity for subsequent formation of the desired ternary nitridosilicate. One possible limitation of this approach is the low boiling point of alkali metals, which moreover form no stable binary nitrides (such as Na, K, Rb, Cs). Therefore, the boiling point of the metal must not be too low as long as open reaction systems are employed. Otherwise, the metal will evaporate before reaction with silicon diimide has started. Similar to the formation of  $\text{Si}_3\text{N}_4$  whiskers, a vapor-solid (VS),<sup>[21]</sup> vapor–liquid–solid (VLS),<sup>[22]</sup> or liquid–solid (LS) mechanism has been assumed for the formation of nitridosilicates.<sup>[20]</sup> A specially developed radio-frequency furnace, used for the inductive heating of the crucibles containing the reaction mixture, is advantageous for obtaining high yields and purities in these reactions (Figure 1).

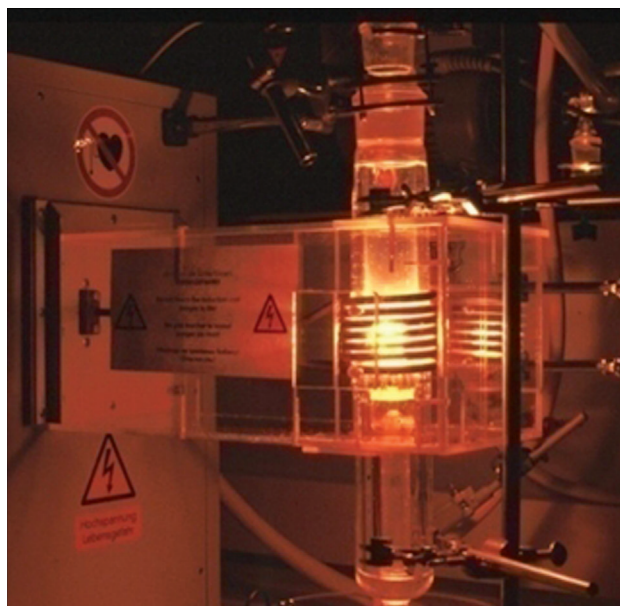


**Figure 1.** Radio-frequency furnace during inductive heating of a tungsten crucible.



Sandro Pagano, born 1981 in Munich, studied chemistry at the University of Munich (LMU) and received his PhD with Wolfgang Schnick in 2009 with a thesis covering organometallic precursor chemistry and leading to innovative approaches to new nitridosilicates. Since mid 2010 he has been working in the chemical industry.

Preparative amounts of nitridosilicates as coarsely crystalline single-phase products are accessible by this procedure in short reaction times. This technique allows very fast heating and high quenching rates ( $>200^\circ\text{C min}^{-1}$ ) of the high-temperature products. For the selection of the crucible materials (for example, tungsten, tantalum, graphite), specific properties, such as chemical inertness and electronic conductivity at high temperatures, have to be considered. Other synthetic approaches have also been reported, for example, the synthesis of  $\text{Sr}_2\text{Si}_3\text{N}_8$  seems possible at temperatures of about 1400–1500°C using the method of carbothermal reduction and nitridation (CRN) of oxides.<sup>[23]</sup> However, the CRN approach may lead to a considerable amount of residual carbon within the synthesized products, possibly influencing material properties.

## 2.2. Flux Methods and Precursor Routes

Recently, novel synthetic approaches to (oxo)nitridosilicates at lower temperatures (<1200°C) have been reported. A flux technique utilizing metallic sodium afforded the synthesis of  $\text{Ba}_5\text{Si}_2\text{N}_6$  at surprisingly low temperatures (ca. 760°C).<sup>[24]</sup> The employment of liquid sodium as a fluxing agent and decomposition of sodium azide as nitrogen source also resulted in the synthesis and structural elucidation of the nitridosilicates  $\text{MSiN}_2$  ( $\text{M} = \text{Ca}, \text{Sr}, \text{Ba}$ ).<sup>[25]</sup> However, limitations occur owing to the boiling point of the flux or the use of closed reaction systems (such as tantalum ampoules) hampering large-scale processing. Recently, a modified flux approach for the synthesis of nitridosilicates utilizing liquid lithium was reported. The reactions were conducted in closed tantalum crucibles at temperatures of about 900°C. The ability of liquid lithium to dissolve a variety of metals,<sup>[26]</sup> inorganic salts, and even complex anions (for example  $[\text{CN}_2]^{2-}$ )<sup>[27]</sup> opened the door to a number of new nitridosilicates.<sup>[28,29]</sup> Crucial for syntheses of nitrides in liquid alkali metals seems to be a significant solubility of nitrogen, which is even enhanced when alkaline earth metals are added.<sup>[28]</sup>

Ammonothermal approaches at low temperatures (500–700°C) have been successfully applied for the preparation and crystal growth of binary nitrides  $\text{AlN}$  or  $\text{GaN}$ .<sup>[30–32]</sup> By contrast, analogous low-temperature solution-based synthetic approaches leading to multinary nitridosilicates have scarcely been investigated. Recently, the synthesis of  $\text{CaAlSiN}_3$  starting from a presynthesized  $\text{CaAlSi}$  alloy has been reported at temperatures of 500–800°C by reaction in supercritical ammonia and subsequent thermal annealing. Optimized yields have been achieved by addition of  $\text{NaNH}_2$  as a mineralizer.<sup>[33]</sup>

Recently, precursor approaches gained increasing importance in the synthesis of nitridosilicates. The use of microcrystalline metal amide precursors  $\text{M}(\text{NH}_2)_2$  ( $\text{M} = \text{Sr}, \text{Ba}, \text{Eu}$ ) and reaction with silicon diimide yielded  $\text{M}_2\text{Si}_5\text{N}_8$  at temperatures as low as 1150°C.<sup>[34]</sup> These precursors have been synthesized previously by dissolving and reacting the respective metals in supercritical ammonia. The amides have proven to be excellent starting materials for the synthesis of nitridosilicates owing to their high reactivity and thermal

decomposition feasibility, producing solely metal nitrides and imides. Additionally, this ammonothermal approach enabled one-pot synthesis of single-source precursors for nitridosilicates.<sup>[35]</sup> Moreover, these “low-temperature” approaches revealed a major influence upon material properties (for example, particle size and morphology).<sup>[33–35]</sup>

### 3. 1D Nitridosilicates

A variety of distinct phases has been claimed for the system  $\text{Li}_3\text{N}-\text{Si}_3\text{N}_4$ , for example,  $\text{LiSi}_2\text{N}_3$ ,<sup>[36,37]</sup>  $\text{Li}_2\text{SiN}_2$ ,<sup>[37–39]</sup>  $\text{Li}_5\text{SiN}_3$ ,<sup>[5,40]</sup>  $\text{Li}_8\text{SiN}_4$ ,<sup>[37,39]</sup>  $\text{Li}_{18}\text{Si}_3\text{N}_{10}$ , and  $\text{Li}_{21}\text{Si}_3\text{N}_{11}$ .<sup>[39]</sup> From a structural point of view, ternary lithium nitridosilicates have been incompletely characterized, as no detailed structural data can be found in the literature for these compounds, with the exception of  $\text{LiSi}_2\text{N}_3$ <sup>[36]</sup> and  $\text{Li}_2\text{SiN}_2$ <sup>[38]</sup> (see Section 5.1). Lithium nitridosilicates are lithium ion conductors (see Section 7.3), and  $\text{Li}_8\text{SiN}_4$  exhibits the highest lithium ion conductivity in this group of compounds investigated to date.<sup>[39]</sup> This might be due to the fact that  $\text{Li}_8\text{SiN}_4$  is supposed to contain orthosilicate-type non-condensed  $[\text{SiN}_4]^{8-}$  tetrahedra.<sup>[37,39]</sup> However, satisfactory structural data are not available for this compound. To date, the only known orthosilicate-type (oxo)nitridosilicate contains  $[\text{SiN}_3\text{O}]^{7-}$  ions.<sup>[41,42]</sup> Accordingly, group-type silicates made up from edge-sharing  $[\text{Si}_2\text{N}_6]^{10-}$  double tetrahedra (Figure 2a) represent the lowest degree of condensation characterized by single-crystal X-ray diffraction in pure nitridosilicates. Analogous anions have been identified in  $\text{Ca}_5\text{Si}_2\text{N}_6$ ,  $\text{Ca}_7[\text{NbSi}_2\text{N}_9]$ ,<sup>[43]</sup>  $\text{Ba}_5\text{Si}_2\text{N}_6$ ,<sup>[24]</sup> and  $\text{Li}_4\text{M}_3\text{Si}_2\text{N}_6$  with  $\text{M} = \text{Ca}, \text{Sr}$ .<sup>[28,44]</sup> In contrast to oxosilicates, edge-sharing  $[\text{Si}_2\text{N}_6]^{10-}$  double tetrahedra and

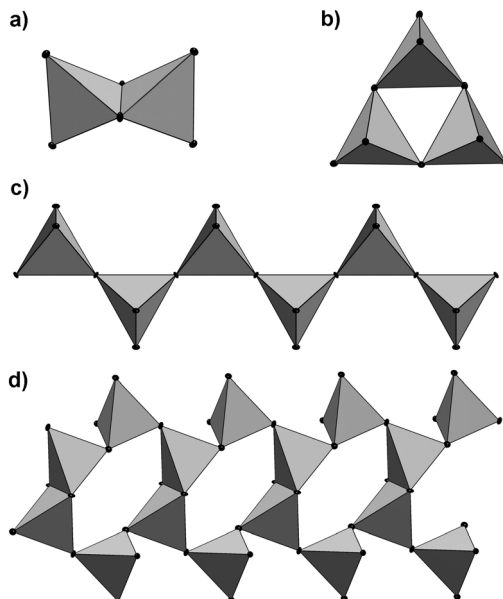


**Figure 2.** a) Isolated, edge-sharing double tetrahedra in  $\text{Ca}_5\text{Si}_2\text{N}_6$ ,  $\text{Ca}_7[\text{NbSi}_2\text{N}_9]$ ,<sup>[43]</sup>  $\text{Ba}_5\text{Si}_2\text{N}_6$ ,<sup>[24]</sup> and  $\text{Li}_4\text{M}_3\text{Si}_2\text{N}_6$  with  $\text{M} = \text{Ca}, \text{Sr}$ .<sup>[28,44]</sup> b) isolated dreier rings in  $\text{Pr}_9\text{Se}_6[\text{Si}_3\text{N}_9]$ .<sup>[45]</sup> c) infinite single-chain in  $\text{Eu}_2\text{SiN}_3$ <sup>[47]</sup> and d) edge-sharing double chain in  $\text{LiCa}_3\text{Si}_2\text{N}_5$ .<sup>[28]</sup>

ring-type ions in  $\text{Pr}_9\text{Se}_6[\text{Si}_3\text{N}_9]$  (Figure 2b) are the only motifs known in nitridosilicates exhibiting a finite dimension.<sup>[45]</sup> Generally speaking, the majority of hitherto investigated nitridosilicates are three-dimensionally condensed framework silicates that have been obtained in high-temperature reactions starting from the respective metals and silicon nitride or silicon diimide ( $\text{Si}(\text{NH})_2$ ). Consequently, the structural variety of chain-like and layer-like structures is still minor compared to oxosilicates.<sup>[1]</sup> Recently, the use of low-temperature approaches led to a considerable number of unprecedented structure types, such as non-branched single-chains observed in  $\text{Li}_5\text{RE}_5\text{Si}_4\text{N}_{12}$  ( $\text{RE} = \text{La}, \text{Ce}$ )<sup>[46]</sup> and  $\text{Eu}_2\text{SiN}_3$ , where the latter exhibits a maximum stretching factor of the chains of 1.0 (Figure 2c).<sup>[47,48]</sup> In  $\text{LiCa}_3\text{Si}_2\text{N}_5$ , two *zweier* single-chains are connected by common edges, forming a double-chain-type arrangement (Figure 2d).<sup>[28,49]</sup>

Interestingly, branched chain-type nitridosilicates  $\text{RE}_5\text{Si}_3\text{N}_9$  with  $\text{RE} = \text{La}, \text{Ce}, \text{Pr}$  and  $\text{La}_{16}[\text{Si}_8\text{N}_{22}][\text{SiON}_3]_2$  (Figure 3a) have been synthesized by high-temperature

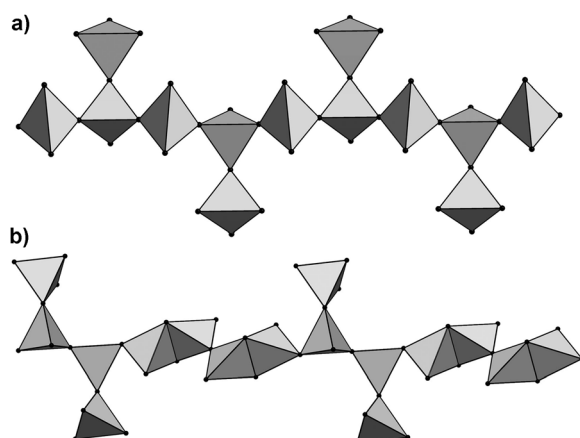


**Figure 3.** a) Branched chain in  $\text{RE}_5\text{Si}_3\text{N}_9$  with  $\text{RE} = \text{La}, \text{Ce}, \text{Pr}$ <sup>[50,51]</sup> and b) branched chain with linking edge-sharing tetrahedra in  $\text{La}_{16}[\text{Si}_8\text{N}_{22}][\text{SiON}_3]_2$ .<sup>[41]</sup>

reactions in a radio-frequency furnace.<sup>[41,50,51]</sup> For  $\text{RE}_5\text{Si}_3\text{N}_9$ , these zipper-like branched chains are intertwined in both directions perpendicular to the chain itself to form a three-dimensionally interlocked structure with the rare earth ions situated between the chains. Apart from non-condensed  $[\text{SiON}_3]^{7-}$  tetrahedra, the structure of  $\text{La}_{16}[\text{Si}_8\text{N}_{22}][\text{SiON}_3]_2$  is made up of both corner-sharing and edge-sharing  $[\text{SiN}_4]$  tetrahedra with additional Q<sup>1</sup>-type  $[\text{SiN}_4]$  groups<sup>[52]</sup> attached to all non-edge-sharing tetrahedra of the chain (Figure 3b). As expected, all less condensed nitridosilicates discussed in this section are moisture sensitive and undergo rapid hydrolysis on exposure to air. This might be due to the missing kinetic prevention of hydrolysis in less condensed nitridosilicates compared to more stable highly condensed representatives.

#### 4. 2D Nitridosilicates

Regarding the isoelectronicity of  $\text{SiO}_2$  and  $[\text{SiN}_2]^{2-}$ , it could be assumed that similar structures exist for the series of nitridosilicates  $\text{MSiN}_2$  with  $\text{M} = \text{Zn}, \text{Mn}, \text{Be}, \text{Mg}, \text{Ca}, \text{Sr}, \text{Ba}$ .<sup>[25,53-58]</sup> However, owing to the more varied connectivity patterns of  $[\text{SiN}_4]$  tetrahedra (vertex sharing, edge sharing,  $\text{N}^{[1]}, \text{N}^{[2]}, \text{N}^{[3]}$ , and even ammonium-type  $\text{N}^{[4]}$ ) compared to  $[\text{SiO}_4]$  tetrahedra (only corner sharing,  $\text{O}^{[1]}, \text{O}^{[2]}$ ), compounds of the formula type  $\text{MSiN}_2$  exhibit alternative structures with a remarkable diversity. The larger ions  $\text{Sr}^{2+}$  and  $\text{Ba}^{2+}$  seem to favor layer-like structures,<sup>[25]</sup> whereas  $\text{MSiN}_2$  with  $\text{M} = \text{Zn}, \text{Mn}, \text{Be}, \text{Mg}$ , or  $\text{Ca}$  represent framework silicates (see Section 5.1). The structures of  $\text{SrSiN}_2$  and  $\text{BaSiN}_2$  are depicted in Figure 4. Pairs of  $[\text{SiN}_4]$  tetrahedra share edges to form “bowtie”  $[\text{Si}_2\text{N}_6]$  units, as previously identified in  $\text{M}_5\text{Si}_2\text{N}_6$  ( $\text{M} = \text{Ca}, \text{Ba}$ ).<sup>[24,43]</sup> These units condense by vertex sharing to form puckered two-dimensional sheets surrounded by cations. Accordingly,  $\text{SrSiN}_2$  and  $\text{BaSiN}_2$  are new types of layered silicates that have no analogues in oxosilicate chemistry.

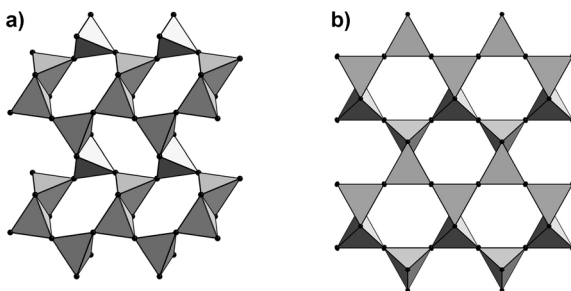


**Figure 4.** Layer-like structures of a)  $\text{SrSiN}_2$  viewed along  $[100]$  and b)  $\text{BaSiN}_2$  viewed along  $[010]$ .<sup>[25]</sup>

The structure of  $\text{SrSiN}_2$  is closely related to that of  $\text{BaSiN}_2$ , but apparently, decreasing the size of the alkaline earth ion from  $\text{Ba}^{2+}$  to  $\text{Sr}^{2+}$  causes distortion of the layers of corner-linked  $[\text{Si}_2\text{N}_6]$  units while lowering the symmetry.<sup>[25]</sup> Recently, three-dimensionally condensed high-pressure modifications of  $\text{SrSiN}_2$  and  $\text{BaSiN}_2$  have been predicted by density-functional methods.<sup>[59]</sup>

The oxonitridosilicate  $\text{CaSi}_2\text{O}_2\text{N}_2$  exhibits an unexpected structure. According to the empirical formula and the respective degree of condensation of  $\kappa = 1/2$ , a three-dimensional framework structure of corner-sharing  $[\text{SiX}_4]$  tetrahedra ( $\text{X} = \text{O}, \text{N}$ ) would be expected. However,  $\text{CaSi}_2\text{O}_2\text{N}_2$  is a layer silicate composed of  $[\text{SiON}_3]$  tetrahedra of the type  $\text{Q}^3$ .<sup>[60]</sup> The unusual composition of the corrugated layer anion  $[\text{Si}_2\text{O}_2\text{N}_2]^{2-}$  originates from the fact that in this compound each N atom, unlike O in oxosilicates, connects three neighboring Si tetrahedron centers ( $\text{N}^{[3]}$ ), whereas the O atoms are exclusively terminally bound to Si ( $\text{O}^{[1]}$ ). The  $[\text{Si}_2\text{O}_2\text{N}_2]^{2-}$  layers in  $\text{CaSi}_2\text{O}_2\text{N}_2$  are assembled from condensed *dreier* rings, a building unit which is unknown in purely oxidic layer silicates and very rare in highly condensed oxosilicates (see Figure 5). The closely related (but not isotopic) structure of  $\text{MSi}_2\text{O}_2\text{N}_2$  ( $\text{M} = \text{Eu}, \text{Sr}$ ) exhibits similar

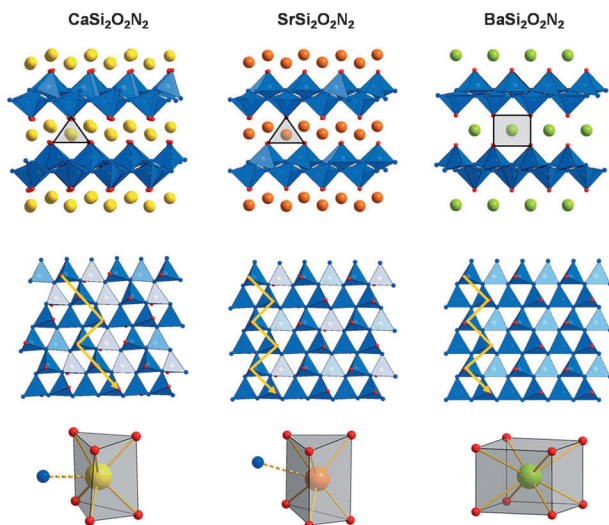


**Figure 5.** Crystal structures of  $\text{MSi}_2\text{O}_2\text{N}_2$  with  $\text{M} = \text{Ca}, \text{Sr}, \text{Ba}$ . Top: Viewed along the silicate layers; middle: *dreier* and *zweier* single chains indicated by arrows viewed perpendicular to the silicate layers (tetrahedra with vertices up dark blue, with vertices down light blue); bottom: coordination of the metal sites to O (red) and N (blue).

metal positions but different silicate layers with analogous O/N ordering.<sup>[61,62]</sup> The layers differ in the up/down sequence of the  $[\text{SiON}_3]$  tetrahedra. In contrast,  $\text{BaSi}_2\text{O}_2\text{N}_2$  exhibits a silicate layer topology similar to  $\text{SrSi}_2\text{O}_2\text{N}_2$  but with different metal coordination sites (Figure 5).<sup>[63]</sup> Nevertheless, mixed solid-solution series have been synthesized, exhibiting promising luminescence properties upon doping with  $\text{Eu}^{2+}$  (see Section 7.5).<sup>[64]</sup> The structural relationship between the mineral sinoite ( $\text{Si}_2\text{N}_2\text{O}$ ) and  $\text{SrSi}_2\text{O}_2\text{N}_2$  can be illustrated by a formal topochemical intercalation of  $\text{SrO}$  into sinoite.<sup>[60]</sup>

The formal substitution of further O into the layers of highly condensed *dreier* rings in  $\text{MSi}_2\text{O}_2\text{N}_2$  type compounds leads to elimination of tetrahedra and partial enlargement of the ring sizes; the layer-like structure is conserved but additional *sechser* rings are formed. Note that the so-formed bridging sites  $\text{X}^{[2]}$  are exclusively occupied by oxygen in accordance with Pauling's second rule (Figure 6a). Accordingly, the nitridosilicate substructure of  $\text{M}_3\text{Si}_6\text{O}_9\text{N}_4$  ( $\text{M} = \text{Ba}$ ,

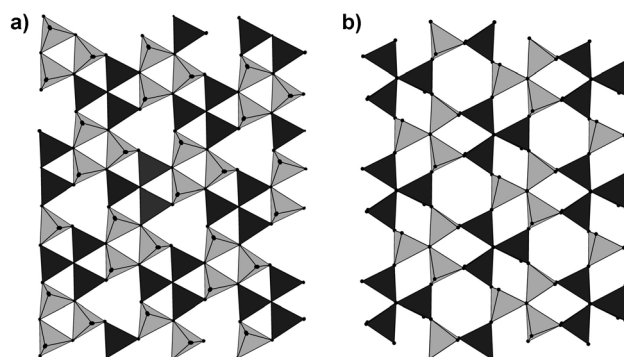


**Figure 6.** a) Layer-like structure of  $\text{M}_3\text{Si}_6\text{O}_9\text{N}_4$  with  $\text{M} = \text{Ba}, \text{Eu}$  and b)  $\text{M}_3\text{Si}_6\text{O}_{12}\text{N}_2$  with  $\text{M} = \text{Sr}, \text{Ba}, \text{Eu}$ . Tetrahedra with vertices up are illustrated in light gray and those with vertices down in dark gray.

$\text{Eu}^{[65]}$  is related topologically to the structure of  $\text{CaSi}_2\text{O}_2\text{N}_2$  by omitting tetrahedra in an ordered fashion.

In contrast, the crystal structure of layered  $\text{M}_3\text{Si}_6\text{O}_{12}\text{N}_2$  ( $\text{M} = \text{Sr}, \text{Ba}, \text{Eu}$ ; Figure 6b) can be derived from the structure of  $\beta\text{-Si}_3\text{N}_4$ .<sup>[66,67]</sup> In silicon nitride, isosteric  $\text{Si}_6\text{N}_{14}$  layers are linked in the third dimension through  $[\text{SiN}_4]$  tetrahedra. A formal derivation of the structure of  $\text{M}_3\text{Si}_6\text{O}_{12}\text{N}_2$  from that of  $\beta\text{-Si}_3\text{N}_4$  can be achieved by separation of the  $\text{Si}_6\text{N}_{14}$  layers in  $\beta\text{-Si}_3\text{N}_4$  and subsequent intercalation of metal ions. Oxide ions that are not connected to Si were found in the oxonitridosilicate oxide  $\text{Ce}_4[\text{Si}_4\text{O}_4\text{N}_6]\text{O}$ , which is built up from large complex tetrahedral cations  $[\text{Ce}_4\text{O}]^{10+}$  and an anionic polymeric network  $[\text{Si}_4\text{O}_4\text{N}_6]^{10-}$  formed by exclusively vertex-sharing  $[\text{SiON}_3]$  tetrahedra.<sup>[68]</sup> Though this compound is cubic, its  $[\text{Si}_4\text{O}_4\text{N}_6]^{10-}$  network can be classified as a layer silicate with a molar ratio  $\text{Si:(O,N)} = 2:5$ . In this specific case, a hyperbolically corrugated topology of the layers is observed, which has been correlated to periodic nodal surface representatives. The periodic nodal surface  $FY_{xxx}$  envelops the large tetrahedral cationic complexes  $[\text{Ce}_4\text{O}]^{10+}$  (see Figure 7).

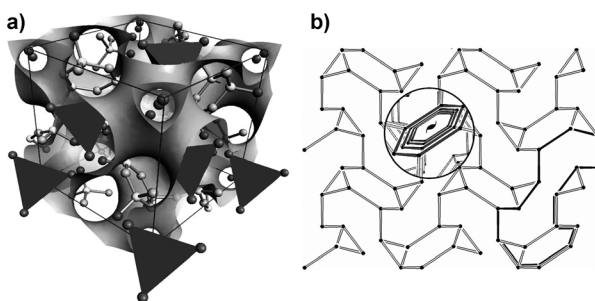


**Figure 7.** a) Crystal structure of  $\text{Ce}_4[\text{Si}_4\text{O}_4\text{N}_6]\text{O}$  viewed along [111]. The periodic nodal surface  $FY_{xxx}$  envelops the large tetrahedral cationic complexes  $[\text{Ce}_4\text{O}]^{10+}$  (dark gray). b) Topological representation of the layer-like structure in  $\text{Ce}_4[\text{Si}_4\text{O}_4\text{N}_6]\text{O}$  (only the Si tetrahedral centers are depicted and connected to each other), viewed along [100]. The network contains small  $\text{Si}_3\text{N}_3$  rings, large  $\text{Si}_{15}\text{N}_{15}$  rings (emphasized by bold lines), and infinite  $2_1$  helices of alternating Si and N atoms running along [100].<sup>[68]</sup>

## 5. 3D Nitridosilicates

### 5.1. Tectosilicates

Silicon nitride is one of the most important non-oxidic ceramic materials. With respect to its sintering properties, the high-pressure behavior of  $\alpha$ - and  $\beta\text{-Si}_3\text{N}_4$  is of particular interest, and it has been investigated over a wide range of pressure and temperature. In 1999, a new spinel-type polymorph of  $\text{Si}_3\text{N}_4$  was reported ( $c\text{-Si}_3\text{N}_4$ ,  $\gamma\text{-Si}_3\text{N}_4$ ), prepared by treating the low-pressure polymorphs or by direct synthesis from the elements under high-pressure (between 10 to 13 GPa) and high-temperature (1800 °C) conditions.<sup>[69]</sup> Furthermore,  $\gamma\text{-Si}_3\text{N}_4$  was also reported to occur as a result of shock-wave treatment of low-pressure silicon nitride polymorphs.<sup>[70]</sup> In  $\gamma\text{-Si}_3\text{N}_4$ , two thirds of the silicon atoms are octahedrally coordinated and one third remains tetrahedrally coordinated,

resulting in solely four-fold crosslinking ammonium-type  $\text{N}^{[4]}$  atoms. According to the formula  $(\text{Si}^{[6]})_2(\text{Si}^{[4]}\text{N}_4)$ , this high-pressure polymorph can be classified as a silicon nitridosilicate.<sup>[1,2]</sup> To further elucidate the relationship between the crystal structure and the mechanical and thermal properties of  $\gamma\text{-Si}_3\text{N}_4$ , extensive first-principles calculations were carried out.<sup>[71-74]</sup>

As already mentioned, the series of nitridosilicates  $\text{MSiN}_2$  exhibits an unexpected structural diversity. Nevertheless, compounds  $\text{MSiN}_2$  with  $\text{M} = \text{Zn}, \text{Be}, \text{Mg}, \text{Mn}$  crystallize isotropically in a three-dimensional network with vertex-sharing  $[\text{SiN}_4]$  tetrahedra, forming condensed  $[\text{Si}_6\text{N}_6]$  ring structures building up a cation-ordered wurtzite-type structure (see Figure 8).<sup>[53-58]</sup> Similar structures have been found in  $\text{LiSi}_2\text{N}_3$ ,  $\text{Li}_2\text{SiO}_3$ , and silicon nitride imide  $\text{Si}_2\text{N}_2(\text{NH})$ . The

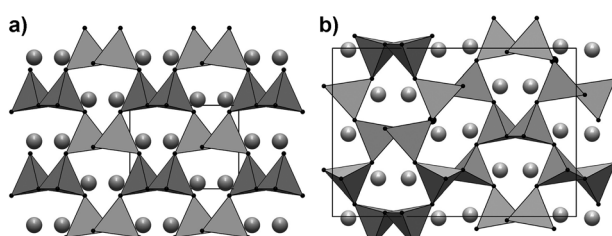


**Figure 8.** a) Wurtzite-derived structure of  $\text{MgSiN}_2$ <sup>[80]</sup> compared with b) the cristobalite-derived structure of  $\text{CaSiN}_2$ .<sup>[25]</sup>

latter compound has been synthesized by ammonothermal methods.<sup>[36,75,76]</sup> In both  $\text{LiSi}_2\text{N}_3$  and  $\text{Si}_2\text{N}_2(\text{NH})$ , parallel layers of condensed  $[\text{Si}_6\text{N}_6]$  rings connected through bridging nitrogen atoms can be observed, which is analogous to  $\text{Si}_2\text{N}_2\text{O}$  or  $\text{SiPN}_3$ .<sup>[77,78]</sup>  $\text{Li}^+$  ions in  $\text{LiSi}_2\text{N}_3$  occupy the remaining tetrahedral sites, completing the wurtzite structure. Reactions of  $\text{NaNH}_2$  and  $\text{Si}_3\text{N}_4$  yielded the isotopic compound  $\text{NaSi}_2\text{N}_3$ .<sup>[79]</sup>

In the past few years, several attempts have been reported to determine the crystal structure of  $\text{Li}_2\text{SiN}_2$ , a promising lithium-ion-conducting material.<sup>[80-82]</sup> Recently, the structure was solved unequivocally from single-crystal X-ray diffraction data.<sup>[38]</sup> The nitridosilicate network is built up from super-tetrahedra (heteroadamantane groups  $[\text{Si}_4\text{N}_6]\text{N}_{4/2}$ ) made up of vertex-sharing tetrahedra forming two interpenetrating cristobalite analogous nets (Figure 9). The asymmetric unit of  $\text{Li}_2\text{SiN}_2$  consists of one  $[\text{Si}_4\text{N}_6]\text{N}_{4/2}$  group and eight symmetrically independent  $\text{Li}^+$  sites. Short  $\text{Li-Li}$  distances and coordination numbers 3 and 5 for  $\text{Li}^+$  allowed possible  $\text{Li}^+$  pathways to be considered for this material.<sup>[38]</sup>

The structure of  $\text{CaSiN}_2$  contains vertex-sharing  $[\text{SiN}_4]$  tetrahedra, as already mentioned above (see Figure 8). The tetrahedra are linked to form a three-dimensional stuffed cristobalite-type framework that is isostructural with that of  $\text{KGaO}_2$ . The arrangement of the vertex-linked tetrahedra in  $\text{CaSiN}_2$  is the D1-type tilting distortion variant of the idealized C9-type  $\beta$ -cristobalite framework.<sup>[83]</sup> Figure 8 compares the structure of  $\text{CaSiN}_2$  with that of  $\text{MgSiN}_2$ , showing that the orientation of the  $[\text{SiN}_4]$  tetrahedra in  $\text{MgSiN}_2$  results in a non-centrosymmetric structure, as found for the wurtzite archetype. Recently, density-functional calculations proposed

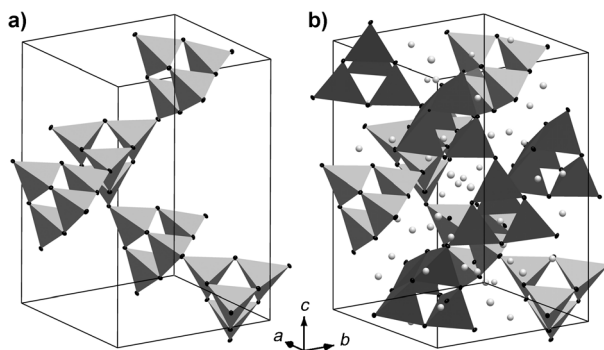


**Figure 9.** a) One branch of the  $[Si_4N_6]N_{4/2}$  network of  $Li_2SiN_2$ . b) Crystal structure of  $Li_2SiN_2$ ;  $[SiN_4]$  units are depicted as closed gray polyhedra, N black spheres,  $Li^+$  gray spheres.<sup>[38]</sup>

several hitherto unknown high-pressure polymorphs of  $MSiN_2$  with  $M = Be, Mg, Ca$ .<sup>[84]</sup>

The quaternary lithium alkaline earth nitridosilicates  $Li_2MSi_2N_4$  with  $M = Ca, Sr$  form an established network structure.<sup>[85]</sup> In this case, the structure is closely related to that of  $BaAl_2S_4$ ,  $BaGa_2S_4$ , and the high-pressure modifications of the borates  $MB_2O_4$  ( $M = Ca, Sr$ ), which are reported to crystallize in *Net 39*.<sup>[86–88]</sup> The cubic structure is built up from exclusively vertex-sharing  $[SiN_4]$  tetrahedra forming a three-dimensional network comprising the alkaline earth and lithium ions in the voids. *Dreier* rings of  $[SiN_4]$  tetrahedra are connected by vertices, forming *siebener* rings (Figure 10).

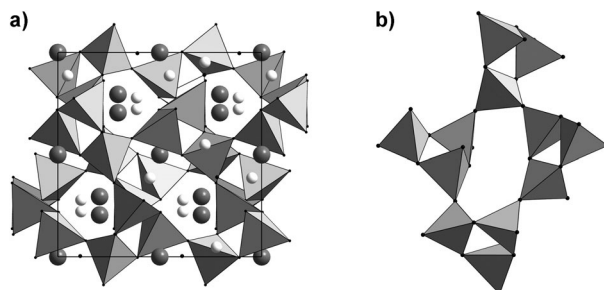


**Figure 10.** Crystal structure of  $Li_2MSi_2N_4$  with  $M = Ca, Sr$ . a) Viewed along  $[100]$ . b) Building unit of the Si/N substructure of  $Li_2MSi_2N_4$ . The  $[SiN_4]$  tetrahedra form *Dreier* rings, four of them build up *siebener* rings.

The family of  $M_2Si_5N_8$  with  $M = Ca, Sr$ , or  $Ba$  (known as the 2-5-8 materials) is a prominent example of nitridosilicates, because upon doping with  $Eu^{2+}$ , they are used industrially in pc-LEDs as highly efficient red-to-orange emitting luminescent materials (see Section 7.5).<sup>[15,89]</sup>  $M_2Si_5N_8$  with  $M = Sr, Ba$ ,<sup>[90]</sup> and  $Eu$ <sup>[91]</sup> crystallize isotropically in the space group  $Pmn2_1$ . The crystal structure is based on a network of corner-sharing  $[SiN_4]$  tetrahedra in which half of the nitrogen atoms connect two ( $N^{[2]}$ ) and the other half connect three neighboring Si atoms ( $N^{[3]}$ ). The  $[SiN_4]$  tetrahedra form corrugated layers of highly condensed *Dreier* rings with  $N^{[3]}$  atoms. These layers are three-dimensionally interconnected through further  $[SiN_4]$  tetrahedra (Figure 11). Carrying the higher formal

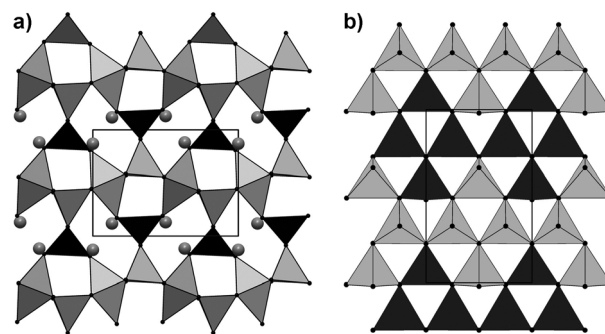


**Figure 11.** Crystal structure of  $M_2Si_5N_8$  ( $M = Sr, Ba, Eu$ ). a) Viewed along  $[100]$ ; corrugated  $[SiN_4]$  layers gray, interconnecting  $[SiN_4]$  tetrahedra black, metal ions gray spheres, nitrogen black spheres. b) View showing layers of condensed *Dreier* rings;  $[SiN_4]$  tetrahedra up (gray), down (black).

charge, the  $N^{[2]}$  atoms mainly coordinate the metal ions, which are situated in channels formed by *sechser* rings.

$Ca_2Si_5N_8$  is composed of vertex-sharing  $[SiN_4]$  tetrahedra exhibiting a similar network compared to  $M_2Si_5N_8$  ( $M = Sr, Ba, Eu$ ) in which half of the nitrogen atoms connect two and the other half connect three silicon atoms. However, it crystallizes in the monoclinic space group  $Cc$  and differs in the distribution of the Si/N ring sizes. Furthermore, significantly less corrugated layers have been observed compared to  $M_2Si_5N_8$  ( $M = Sr, Ba, Eu$ ; Figure 12).

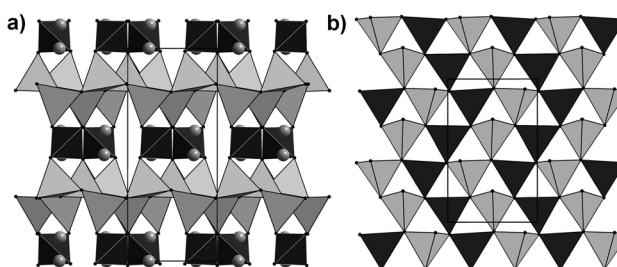


**Figure 12.** Crystal structure of  $Ca_2Si_5N_8$ . a) Viewed along  $[100]$ ; corrugated  $[SiN_4]$  layers gray, interconnecting  $[SiN_4]$  tetrahedra black, metal ions gray spheres, nitrogen black spheres. b) View of layer of condensed *Dreier* rings; tetrahedra up (gray), down (black).

Although  $Ca_2Si_5N_8$  exhibits a rigid three-dimensional network, a high-pressure (HP) phase transition has recently been observed. In this context, HP- $Ca_2Si_5N_8$  has been obtained by means of high-pressure high-temperature synthesis utilizing the multi-anvil technique starting from the ambient-pressure phase of  $Ca_2Si_5N_8$ .<sup>[92]</sup> HP- $Ca_2Si_5N_8$  can be described as a centrosymmetric variant of the non-centro-symmetric ambient-pressure modification, exhibiting significantly more strongly corrugated layers of  $[SiN_4]$  tetrahedra (see Figure 13). Even though the structures of ambient-pressure  $Ca_2Si_5N_8$  and HP- $Ca_2Si_5N_8$  are closely related, the phase transformation is reconstructive and occurs nevertheless at quite low temperature and pressure ( $900^\circ C, 6$  GPa). However, the activation energy for the retransformation into

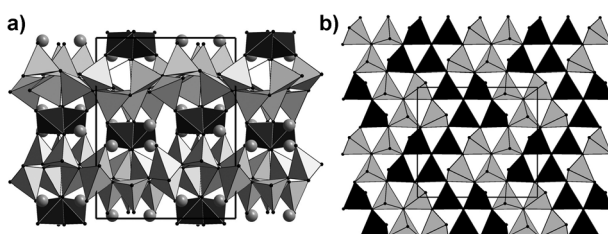


**Figure 13.** Crystal structure of HP-Ca<sub>2</sub>Si<sub>5</sub>N<sub>8</sub>. a) Viewed along [100]; corrugated layer gray, interconnecting [SiN<sub>4</sub>] tetrahedra black, metal ions gray spheres, nitrogen black spheres. b) View showing layer of condensed *dreier* rings; tetrahedra up (gray), down (black).

the ambient-pressure phase is large enough to render HP-Ca<sub>2</sub>Si<sub>5</sub>N<sub>8</sub> metastable at normal pressure.

Solid-solution series of the 2-5-8 phases are also widely known, resulting in a number of compositions (also Al/O incorporation), which upon doping with Eu, Ce, Tb exhibit promising luminescence properties for applications in white pc-LEDs (see Section 7.5).<sup>[93,94]</sup>

LaSi<sub>3</sub>N<sub>5</sub> has been obtained by the reaction of Si<sub>3</sub>N<sub>4</sub> and La<sub>2</sub>O<sub>3</sub> at 2000°C and 725 psi (50 bar) N<sub>2</sub> pressure.<sup>[95]</sup> Nitridation of two-phase alloys RESi<sub>3</sub> led to RESi<sub>3</sub>N<sub>5</sub> with RE = Ce, Pr, Nd.<sup>[96]</sup> The structure is built up exclusively of vertex-sharing [SiN<sub>4</sub>] tetrahedra forming *vierer* rings, which are interconnected by chains of [SiN<sub>4</sub>] tetrahedra, forming a three-dimensional network (Figure 14a). According to the molar ratio of Si:N = 3:5, two fifths of the nitrogen atoms connect three silicon atoms (N<sup>[3]</sup>), whereas three fifths are connected with two silicon atoms (N<sup>[2]</sup>).

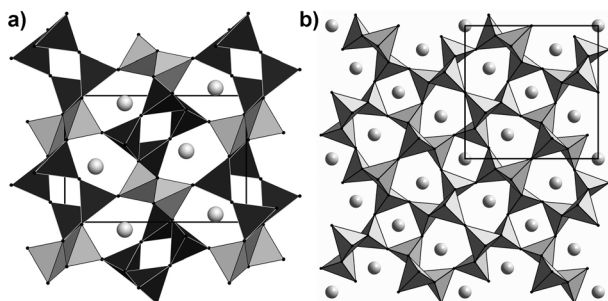


**Figure 14.** a) Crystal structure of LaSi<sub>3</sub>N<sub>5</sub> (viewed along [100]), *vierer* rings dark, interconnecting [SiN<sub>4</sub>] tetrahedra light gray, metal ions gray spheres, nitrogen black spheres. b) Crystal structure of Sm<sub>3</sub>Si<sub>6</sub>N<sub>11</sub> viewed along [001]; [SiN<sub>4</sub>] tetrahedra light gray, metal ions gray spheres, nitrogen black spheres.

Sm<sub>3</sub>Si<sub>6</sub>N<sub>11</sub> was first synthesized from Gaudé et al. starting from SmN and Si<sub>3</sub>N<sub>4</sub>.<sup>[97]</sup> Compounds with the same formula type were further studied comprehensively by Schlieper et al. and Woike et al., who reported synthetic approaches starting from the respective metals and Si(NH)<sub>2</sub>, as well as the reaction of the silicides RESi<sub>2</sub> with N<sub>2</sub>.<sup>[96,98,99]</sup> The three-dimensional network consists of vertex-sharing [SiN<sub>4</sub>] tetrahedra, whereas nine nitrogen atoms form simple Si–N<sup>[2]</sup>–Si bridges and two of them connect three silicon atoms (N<sup>[3]</sup>). This results in layers of *vierer* and *achter* rings of [SiN<sub>4</sub>] tetrahedra, which are

stacked along [001] and connected by double tetrahedra bridging the *achter* rings (Figure 14b). Although BaEu-(Ba<sub>0.5</sub>Eu<sub>0.5</sub>)YbSi<sub>6</sub>N<sub>11</sub> exhibits the same molar ratio regarding the anions [Si<sub>6</sub>N<sub>11</sub>]<sup>9-</sup>, a completely differing network topology was observed.<sup>[100]</sup> This might be due to the appearance of Ba<sup>2+</sup>, Eu<sup>2+</sup>, and Yb<sup>3+</sup> in one and the same compound. The structure consists of two symmetrically independent [N-(SiN<sub>3</sub>)<sub>3</sub>] units that are built up of three [SiN<sub>4</sub>] tetrahedra connected by a shared nitrogen atom (N<sup>[3]</sup>). Further bridging nitrogen atoms N<sup>[2]</sup> establish the three-dimensional nitridosilicate network. With Ba<sub>4-x</sub>Ca<sub>x</sub>Si<sub>6</sub>N<sub>10</sub>O an isotypic compound has been reported, whereas the smaller negative charge of the lattice is balanced exclusively with alkaline earth ions.<sup>[101]</sup>

MSi<sub>7</sub>N<sub>10</sub> (M = Sr, Ba) was the first nitridosilicate with both edge-sharing and corner-sharing [SiN<sub>4</sub>] tetrahedra.<sup>[102,103]</sup> Every fifth nitrogen connects two Si centers (N<sup>[2]</sup>), and the remaining nitrogen atoms bridge three Si atoms (N<sup>[3]</sup>). The vertex-sharing [SiN<sub>4</sub>] tetrahedra are arranged in nearly coplanar, slightly corrugated layers of highly condensed *dreier* rings perpendicular to [010]. Additionally, these layers are bridged by parallel *vierer* single chains along [001] in which every second connection between neighboring [SiN<sub>4</sub>] tetrahedra is through common edges (Figure 15).

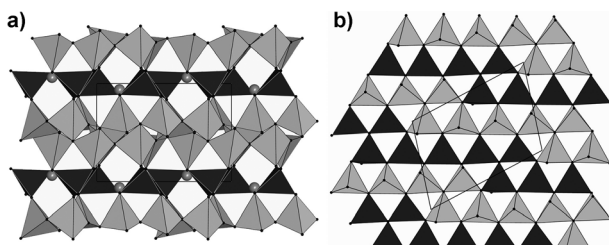


**Figure 15.** Crystal structure of MSi<sub>7</sub>N<sub>10</sub> (M = Sr, Ba). a) Viewed along corrugated [SiN<sub>4</sub>] layers (gray) and interconnected by [SiN<sub>4</sub>] *vierer* single chains (black); metal ions gray spheres, nitrogen black spheres. b) View showing layers of condensed *dreier* rings; [SiN<sub>4</sub>] tetrahedra up (gray), down (black).

Therefore, edge sharing does not seem to compete with vertex sharing, probably owing to the lower ionic bonding character in nitridosilicates, in contrast to the more ionic character of the Si–O bonds in oxosilicates. Within the group of the hitherto known ternary nitridosilicates, MSi<sub>7</sub>N<sub>10</sub> with M = Sr, Ba adopt the most highly condensed ternary framework structure. The molar ratio Si:N = 1:1.43 reaches almost the value of binary Si<sub>3</sub>N<sub>4</sub> (1:1.33).

While the chemistry of oxosilicates is limited to terminal oxygen atoms and simply bridging O<sup>[2]</sup> atoms, nitridosilicates exhibit a much broader range of structural arrangements, as shown in the previous examples. Thus, apart from edge sharing of [SiN<sub>4</sub>] tetrahedra also N<sup>[1]</sup>, N<sup>[2]</sup>, and N<sup>[3]</sup> atoms are known. One rare example of even fourfold coordinating nitrogen atoms is MYbSi<sub>4</sub>N<sub>7</sub> with M = Eu, Sr, Ba)<sup>[91,104,105]</sup> which Si–N network structure is built up from star-shaped [N(SiN<sub>3</sub>)<sub>4</sub>] building blocks. The central nitrogen atoms of these building blocks bridge four neighboring Si atoms (N<sup>[4]</sup>) and thus exhibit ammonium-type character (Figure 16). By

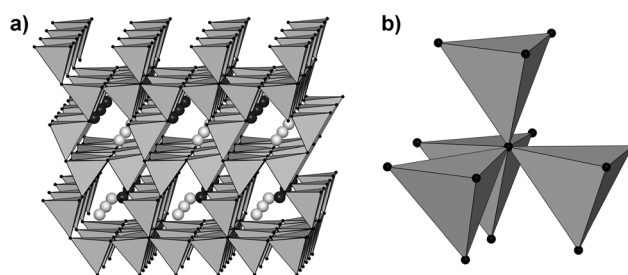


**Figure 16.** Crystal structure of  $\text{MYbSi}_4\text{N}_7$  ( $\text{M} = \text{Eu}, \text{Sr}, \text{Ba}$ ). a) Viewed along sheets of highly condensed *dreier* rings [100];  $[\text{SiN}_4]$  layers gray, metal ions large black and light gray spheres, nitrogen small black spheres. b)  $[\text{N}(\text{SiN}_3)_4]$  building block with  $\text{N}^{[4]}$ .

connecting these groups through common  $\text{N}^{[2]}$  atoms, a stacking variant of the wurtzite analogous aluminum nitride structure is formed. Systematic elimination of tetrahedra from this arrangement along [100] leads to the formation of *sechser* ring channels, containing  $\text{M}^{2+}$  and  $\text{Yb}^{3+}$  ions (Figure 16). More recently, Li et al. reported the isostructural compound  $\text{EuYSi}_4\text{N}_7$ <sup>[106]</sup> furthermore,  $\text{SiAlON}$  substitutional variants  $\text{MRE}[\text{Si}_{4-x}\text{Al}_x\text{O}_x\text{N}_{7-x}]$  with  $\text{M} = \text{Eu}, \text{Sr}, \text{Ba}$  and  $\text{RE} = \text{Ho} - \text{Yb}$  have been reported by Lieb et al.<sup>[107]</sup>

The formal substitution of four-fold coordinated nitrogen by carbon in nitridosilicates of formula type  $\text{MYbSi}_4\text{N}_7$  has also been reported. Reaction of the respective lanthanide metals with carbon and  $\text{Si}(\text{NH})_2$  led to isostructural compounds  $\text{RE}_2[\text{Si}_4\text{N}_6\text{C}]$  with  $\text{RE} = \text{Y}, \text{Tb}, \text{Ho}, \text{Er}$ .<sup>[108–110]</sup> The structure contains a condensed network of corner-sharing, star-like  $[\text{C}(\text{SiN}_3)_4]$  units. Apparently, the range of composition of nitridosilicates can be extended by the substitution of N by C, leading to carbidonitridosilicates.

Apart from remarkable structural features, such as edge sharing of  $[\text{SiN}_4]$  tetrahedra and four-fold coordinated nitrogen atoms, reduced nitridosilicates with Si–Si bonds (with oxidation number Si < 4) are also known. Nitrides of formula type  $\text{MSi}_6\text{N}_8$  with  $\text{M} = \text{Sr}, \text{Ba}$  are partially reduced compounds with a silicate substructure containing Si in oxidation states + III and + IV.<sup>[111,112]</sup> The framework structure differs significantly from any other known silicate structure, as it does not comprise a strictly alternating sequence of Si and X atoms ( $\text{X} = \text{O}, \text{N}$ ). Actually,  $[\text{SiN}_4]$  tetrahedra and disilane analogous  $\text{N}_3\text{Si}-\text{SiN}_3$  entities, in which each nitrogen atom bridges three silicon atoms, occur in  $\text{MSi}_6\text{N}_8$  with  $\text{M} = \text{Sr}, \text{Ba}$ . Therefore, it contains additional Si–Si single bonds (235.2(2) pm), similar to the covalent Si–Si single bond in elemental silicon (Figure 17a,c). From the reaction of  $\text{BaCO}_3$  and  $\text{Si}(\text{NH})_2$ , the oxonitridosilicate  $\text{BaSi}_6\text{N}_8\text{O}$  was obtained, which crystallizes in a structure which is homeotypic with that of  $\text{MSi}_6\text{N}_8$ . Comparing the tetrahedra frameworks of the two compounds, it is evident that in the oxonitridosilicate, an oxygen atom is formally inserted into the Si–Si bond, thus leading to two vertex sharing tetrahedra. Moreover, this results in the formation of exclusively tetravalent silicon with  $[\text{SiON}_3]$  tetrahedra along with  $[\text{SiN}_4]$  tetrahedra (Figure 17b,d).  $\text{SiAlON}$   $\text{Sr}_2\text{Al}_x\text{Si}_{12-x}\text{N}_{16-x}\text{O}_{2+x}$  ( $x \approx 2$ ) exhibits an isotopic structure, therefore the analogous silicon atoms are also bridged by oxygen atoms.<sup>[113]</sup>

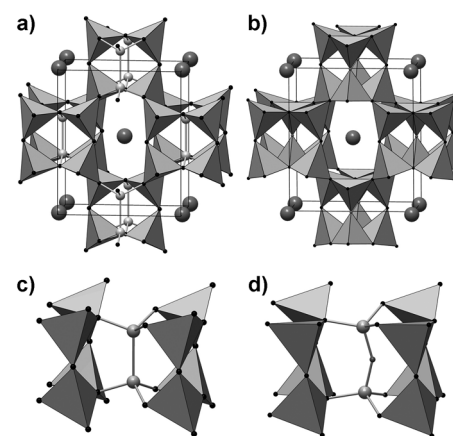


**Figure 17.** Comparison of the crystal structures of a)  $\text{MSi}_6\text{N}_8$  ( $\text{M} = \text{Sr}, \text{Ba}$ ) and b)  $\text{BaSi}_6\text{N}_8\text{O}$ . Viewed along [001]. c,d) Comparison of the silicon surroundings in c)  $\text{MSi}_6\text{N}_8$  ( $\text{M} = \text{Sr}, \text{Ba}$ ) and d)  $\text{BaSi}_6\text{N}_8\text{O}$ .

## 5.2. *SiAlNs*

Apart from oxosilicates, nitridosilicates, and oxonitridosilicates, there is an extension that further augments the structural diversity in silicate chemistry. Partial formal substitution of silicon by aluminum leads to nitridoalumosilicates, which have been scarcely investigated to date.

Wurtzite-type related structures for nitridoalumosilicates have been reported for  $\text{MAISiN}_3$  with  $\text{M} = \text{Be}, \text{Mg}, \text{Mn}$  and  $\text{Ca}$ <sup>[114]</sup> with structures that are closely related to that of  $\text{LiSi}_2\text{N}_3$  (see Section 3.1).<sup>[115]</sup>  $\text{CaAlSiN}_3$  in particular, the most recently discovered Sr analogue and the solid-solution series (Ca,Sr)- $\text{AlSiN}_3$ , have been intensively investigated as host lattices to be used in white light pc-LEDs when doped with  $\text{Eu}^{2+}$  or  $\text{Ce}^{3+}$  (see Section 7.5).  $\text{CaAlSiN}_3$  is built up of a three-dimensional network structure comprising  $[(\text{Si}, \text{Al})\text{N}_4]$  tetrahedra where one third of the nitrogen atoms connect two Si ( $\text{N}^{[2]}$ ) and the remaining two thirds ( $\text{N}^{[3]}$ ) connect three tetrahedral centers (Figure 18). The Al and Si atoms are randomly distributed on the same tetrahedral sites forming  $(\text{Si}, \text{Al})_6\text{N}_6$  rings. The structure of  $\text{CaAlSiN}_3$  can be regarded as a superstructure variant of the wurtzite-type binaries  $\text{AlN}$  or  $\text{GaN}$ .

The nitridoalumosilicate  $\text{SrAlSi}_4\text{N}_7$  contains a highly condensed network structure built up of  $[\text{SiN}_4]$  and  $[\text{AlN}_4]$  tetrahedra.<sup>[116]</sup>  $\text{SrAlSi}_4\text{N}_7$  (no structural relation to  $\text{MYbSi}_4\text{N}_7$ )

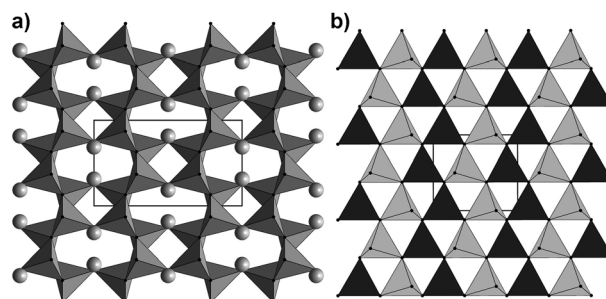


**Figure 18.** Structure of  $\text{CaAlSiN}_3$ . a) Viewed along [001], Ca light gray spheres,  $[\text{SiN}_4]$  tetrahedra gray. b) View showing layers of condensed *dreier* rings;  $[\text{SiN}_4]$  tetrahedra up (gray), down (black).

(M = Sr, Ba; see Section 5.1) is a nitridoalumosilicate featuring infinite one-dimensional chains of edge-sharing tetrahedra that are most probably centered solely by aluminum. Particularly interesting is the geometric situation inside these chains, which are almost linear. These *trans*-linked chains are connected exclusively through common corners with the highly corrugated  $[\text{SiN}_4]$  layers forming a three-dimensional network (Figure 19), pervaded with channels alongside the chains. The channels host two different  $\text{Sr}^{2+}$  positions that are coordinated by irregular polyhedra made up of six or eight nitrogen atoms.

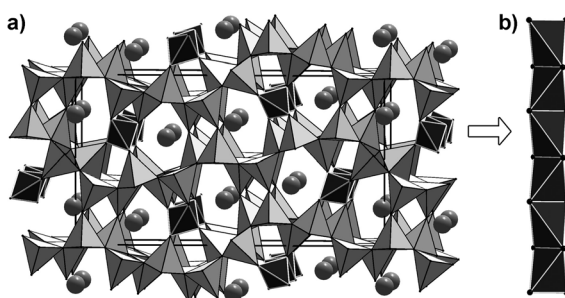


**Figure 19.** a) Structure of  $\text{SrAlSi}_4\text{N}_7$ , viewed along [001]; chains of edge-sharing tetrahedra are marked in black, Sr gray spheres,  $[\text{SiN}_4]$  tetrahedra light gray. b) Strand of edge-sharing tetrahedra viewed along [100].

$\text{Ba}_2\text{AlSi}_5\text{N}_9$  is a type of network structure built up of  $[(\text{Si}, \text{Al})\text{N}_4]$  tetrahedra, which are connected by bridging  $\text{N}^{[2]}$  and  $\text{N}^{[3]}$  atoms.<sup>[117]</sup> It consists of highly condensed layers of exclusively vertex-sharing *dreier* rings exhibiting an unusual up/down sequence of the tetrahedra, compared to layer silicates such as  $\text{MSi}_2\text{O}_2\text{N}_2$  (M = Ca, Sr, Ba, Eu; see Section 4) and also to partial structures in other frameworks such as  $\text{M}_2\text{Si}_5\text{N}_8$  (M = Ca, Sr, Ba; see Section 5.1). The silicate layers are interconnected by *dreier* rings made up of exclusively vertex-sharing tetrahedra that are condensed through two shared corners, building up one *vierer* ring per pair (see Figure 20). The layers are further interconnected by a second kind of *vierer* rings made up of two vertex-sharing pairs of edge-sharing tetrahedra  $[(\text{Si}, \text{Al})_2\text{N}_6]$  (see Figure 20b,c). This

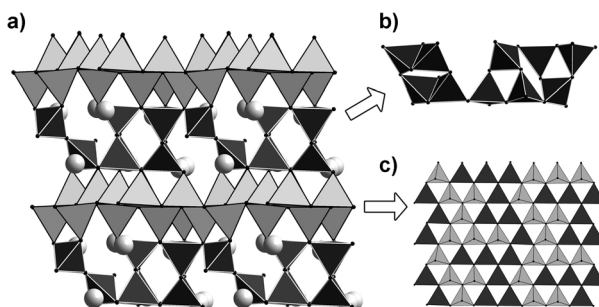


**Figure 20.** a) Structure of  $\text{Ba}_2\text{AlSi}_5\text{N}_9$ , viewed along [100]; interconnecting *dreier* and *vierer* rings black, Ba gray spheres,  $[\text{Al/SiN}_4]$  tetrahedra light gray. b) Interconnecting *dreier* and *vierer* rings. c) View upon layers of condensed *dreier* rings;  $[\text{SiN}_4]$  tetrahedra up (gray), down (black).

kind of *vierer* ring motif is rather unusual and has not been observed in other nitridosilicates to date. However, the nitridogallate  $\text{Sr}_3\text{Ga}_3\text{N}_5$  contains an isoelectronic variant of such *vierer* rings.<sup>[118]</sup> In the resulting voids of the network, there are eight different  $\text{Ba}^{2+}$  sites with coordination numbers between 6 and 10.

Recently, Ottinger et al. reported  $\text{Ca}_5\text{Si}_2\text{Al}_2\text{N}_8$ , which contains a three-dimensional network of both edge- and vertex-connected tetrahedra  $[\text{TN}_4]$  with T = Al, Si.<sup>[114, 119, 120]</sup> The building units are exclusively edge-sharing double tetrahedra  $[\text{T}_2\text{N}_6]$ . Perpendicular to the [001] direction, the  $[\text{Al}_2\text{N}_6]$  units form sheets connected by  $[\text{Si}_2\text{N}_6]$  double tetrahedra with  $\text{N}^{[3]}$  in which the  $[\text{AlN}_4]$  tetrahedra are arranged forming *sechser* rings (see Figure 21).

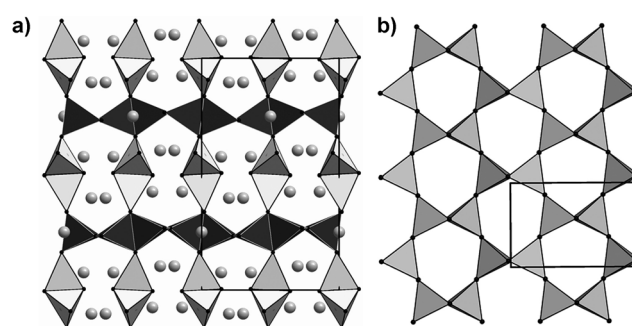


**Figure 21.** a) Structure of  $\text{Ca}_5\text{Si}_2\text{Al}_2\text{N}_8$ , viewed along [010], double tetrahedra of  $[\text{Si}_2\text{N}_6]$  gray,  $[\text{Al}_2\text{N}_6]$  black, Ca gray spheres. b) Layer of edge-sharing  $[\text{Al}_2\text{N}_6]$  units viewed along [001].

Further three-dimensionally condensed SiAlN compounds with more complicated structures are reported for  $\text{Ca}_4\text{SiAl}_3\text{N}_7$ ,<sup>[114, 120]</sup>  $\text{La}_{17}\text{Si}_9\text{Al}_4\text{N}_{33}$ ,<sup>[121]</sup>  $\text{Li}_x\text{Al}_{12-3x}\text{Si}_{2x}\text{N}_{12}$  ( $1 \leq x \leq 3$ ),<sup>[122]</sup> and filled types analogously to the  $\alpha\text{-Si}_3\text{N}_4$  structure.<sup>[123]</sup>

### 5.3. SiAlONs

Oxonitridoalumosilicates (SiAlONs) are related to silicon nitrides or nitridosilicates by partial substitution (Si/N) by (Al/O). For ceramic applications, such SiAlONs have frequently been synthesized by hot-press techniques, and the first members of this class of compounds were obtained from the reaction of  $\text{Si}_3\text{N}_4$  and  $\text{Al}_2\text{O}_3$ .<sup>[9, 124]</sup> From a structural point of view, the latter SiAlONs derive mainly from  $\alpha$ - and  $\beta\text{-Si}_3\text{N}_4$ . However, in the meantime, several SiAlONs with anionic networks and additional cations have also been described. Interestingly, some of them are isotypic with known nitrido- and oxonitridosilicate structures, for example,  $\text{SrErSiAl}_3\text{O}_3\text{N}_4$ <sup>[20]</sup> and  $\text{MRESi}_{4-x}\text{Al}_x\text{O}_x\text{N}_{7-x}$  with M = Eu, Sr, Ba and RE = Ho–Yb<sup>[107]</sup> (both isotypic to  $\text{MYbSi}_4\text{N}_7$  with M = Sr, Ba),<sup>[104, 105]</sup>  $\text{Nd}_3\text{Si}_5\text{AlON}_{10}$ <sup>[125]</sup> (isotypic to  $\text{RE}_3\text{Si}_6\text{N}_{11}$  with RE = La, Ce, Pr, Nd, Sm),<sup>[96, 98, 99]</sup>  $\text{Y}_2\text{Si}_{3-x}\text{Al}_x\text{O}_{3+x}\text{N}_{4-x}$ <sup>[126]</sup> (isotypic to melilite type  $\text{Y}_2\text{Si}_3\text{O}_3\text{N}_4$ ),  $\text{Sr}_2\text{Al}_x\text{Si}_{12-x}\text{N}_{16-x}\text{O}_{2+x}$  with  $x = 2$ <sup>[113]</sup> (isotypic to  $\text{BaSi}_6\text{N}_8\text{O}$ ),<sup>[127]</sup> or  $\text{SrSiAl}_2\text{O}_3\text{N}_2$  (isotypic to  $\text{RESi}_3\text{N}_5$  with RE = La, Ce, Pr, Nd).<sup>[128]</sup>

Whereas other SiAlONs are structurally related to oxosilicates,<sup>[129]</sup> several representatives exhibit unique struc-

ture types, such as  $\text{Sr}_3\text{RE}_{10}\text{Si}_{18}\text{Al}_{12}\text{O}_{18}\text{N}_{36}$  ( $\text{RE} = \text{Ce}, \text{Pr}, \text{Nd}$ ), which consist of a three-dimensional network of vertex-sharing  $[\text{SiON}_3]$ ,  $[\text{AlON}_3]$ , and  $[\text{SiN}_4]$  tetrahedra.<sup>[130]</sup> Typical building blocks of the crystal structure are double *dreier* rings formed by three  $[\text{SiON}_3]$  and three  $[\text{AlON}_3]$  tetrahedra connected by bridging O<sup>2-</sup> atoms (see Figure 22). These

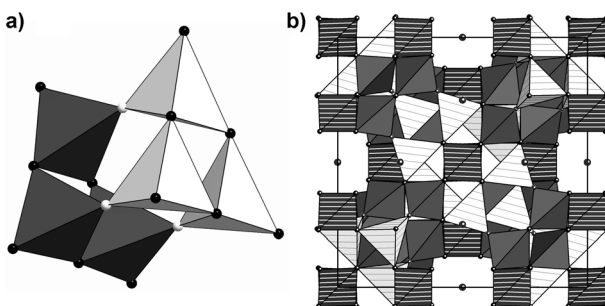


**Figure 22.** a) Double *dreier* rings  $[\text{Si}_3\text{Al}_3\text{O}_3\text{N}_6]$  in  $\text{Sr}_3\text{RE}_{10}\text{Si}_{18}\text{Al}_{12}\text{O}_{18}\text{N}_{36}$  ( $\text{RE} = \text{Ce}, \text{Pr}, \text{Nd}$ ). b) Three-dimensional network in  $\text{Sr}_3\text{RE}_{10}\text{Si}_{18}\text{Al}_{12}\text{O}_{18}\text{N}_{36}$  ( $\text{RE} = \text{Ce}, \text{Pr}, \text{Nd}$ ). The  $[\text{SiON}_3]$  units are depicted in dark gray,  $[\text{AlON}_3]$  as white tetrahedra with gray hatching, and  $[\text{SiN}_4]$  tetrahedra as darkly hatched polyhedra.

double *dreier* rings are further connected through  $[\text{SiN}_4]$  tetrahedra, building up a three-dimensional network incorporating large tetrahedral cations  $[(\text{Sr}/\text{RE})_4\text{O}]$ . In this case a crystallographic differentiation of Si/Al and O/N seemed possible owing to a careful evaluation of single-crystal X-ray data combined with lattice energy calculations and powder neutron-diffraction data.<sup>[130]</sup>

Two-dimensionally ordered anionic structures have been observed in  $\text{Sr}_{10}\text{Sm}_6\text{Si}_{30}\text{Al}_6\text{O}_7\text{N}_{54}$ , which exhibit a capped double-layer structure formed by vertex-sharing  $[\text{SiON}_3]$ ,  $[\text{SiN}_4]$ ,  $[\text{AlON}_3]$ , and  $[\text{AlN}_4]$  tetrahedra building up large channels running along  $[001]$ .<sup>[131]</sup> More complex SiAlON structures are known, for example in  $\text{Sr}_5\text{Al}_{5+x}\text{Si}_{21-x}\text{N}_{35-x}\text{O}_{2+x}:\text{Eu}^{2+}$  (with  $x \approx 0$ ), which exhibits a complex intergrowth structure consisting of highly condensed *dreier* ring layers alternating with *sechser* ring layers that include both vertex- and edge-sharing  $[(\text{Si},\text{Al})(\text{O},\text{N})_4]$  tetrahedra. Both layer types exhibit pseudo-translational symmetry, which leads to a more or less pronounced disorder of the *sechser* ring layers.<sup>[132]</sup> Recently, the SiAlON  $(\text{Sr}_{1-x}\text{Ca}_x)_{(11+16y-25z)/2}(\text{Si}_{1-y}\text{Al}_y)_{16}(\text{N}_{1-z}\text{O}_z)_{25}$  ( $x \approx 0.24$ ,  $y \approx 0.18$ ,  $z \approx 0.19$ )<sup>[133]</sup> was reported in which the anionic part of the structure is built up from highly condensed *dreier* ring layers extending parallel to the  $[100]$  direction and interconnected by common N and O atoms.

This review can give only a small impression of the versatile class of SiAlONs. Generally, the main problem with the experimental characterization of SiAlONs by X-ray diffraction methods is the similarity of the atomic form factors of O and N and of Al and Si, respectively. Consequently, a statistical distribution of Al/Si and N/O is assumed for the majority of published SiAlON structures. However, both difficulties in the preparation of chemically homogeneous samples and the uncertainty associated with the chemical analysis of large samples can limit the validity of

quantitative conclusions in this class of compounds and requires further systematic investigations.

#### 5.4. Zeolite-Like Structures

Nitridosilicates are a significant extension of the broad and varied crystal chemistry of classical oxosilicates, although on a local atomic scale, both oxosilicates and nitridosilicates are made up of analogous and isosteric building blocks, namely  $[\text{SiO}_4]$  and  $[\text{SiN}_4]$  tetrahedra, respectively. Therefore, it is not surprising that apart from many analogous structural motifs, even nitrido-analogous zeolite structures have been found. With regard to the material properties and the high chemical and thermal stability of nitridosilicates, it seems to be intriguing to synthesize zeolite-like microporous network structures made up of  $[\text{SiN}_4]$  tetrahedra. However, at present, nitridosilicates are solely accessible by high-temperature reactions and under such conditions, standard templates known from conventional zeolite syntheses are ineligible. Furthermore, the kinetic control that is typical for template synthesis seems difficult at such high temperatures ( $> 700^\circ\text{C}$ ). The higher charge of  $[\text{SiN}_2]^{2-}$  networks compared to  $\text{SiO}_2$  or  $[\text{SiAlO}_4]^-$  is usually compensated by metal ions. Nitridosilicates exhibiting protonated N-atoms (imido groups) such as  $\text{K}_5\text{Si}_6\text{N}_5(\text{NH})_6$  are rather sensitive to air and scarcely known.<sup>[134,135]</sup> In all zeolite-like nitridosilicates synthesized to date, the cavities are filled by large alkaline earth or lanthanide ions. In some cases, complex anions such as  $[\text{BN}_3]^{6-}$  or  $[\text{CN}_2]^{2-}$  are also incorporated into the networks.<sup>[29,136]</sup> To the best of our knowledge, comprehensive ion exchange typical for classical zeolites has not yet been reported for nitridic zeolites. Nevertheless, (oxo)nitridosilicates can exhibit unprecedented framework structures. The framework density (FD) of such nitridic networks (that is, the number of tetrahedral centers in a volume of  $1000 \text{ \AA}^3$ ) varies in a range typical for classical oxidic zeolites. In the latter class of compounds, FD values range from about 12 to 20.<sup>[137]</sup> It may be noted that typically Si–N bonds are longer than Si–O bonds, which is due to the larger radius of  $\text{N}^{3-}$  compared with  $\text{O}^{2-}$ . Accordingly,  $[\text{SiN}_4]$  tetrahedra and the entire nitridic network are approximately 20% larger in volume as compared to isostructural oxidic networks.<sup>[138]</sup> As a consequence, the FD values of nitridosilicates should be corrected by a factor 1.2 to afford comparable values for the accessible space inside the network. In Table 1, such FD values are compared with two classical zeolites in which fictive  $[\text{SiN}_4]$  values have been calculated. As an example, the same accessible volume as in faujasite would be reached in a nitridic zeolite with  $\text{FD} = 10.2$ .

Oxonitridosilicates  $\text{Ba}_3\text{Si}_3\text{N}_5\text{OCl}$  and  $\text{Ba}_6\text{Si}_6\text{N}_{10}\text{O}_2(\text{CN}_2)$  are zeolites with the *NPO* (nitridophosphate one) framework type.<sup>[29,139]</sup> This network was initially claimed as a possible  $\text{SiO}_2$  structure type, which, however, has not been observed for  $\text{SiO}_2$  or oxosilicates as yet. The first representatives of this topology were oxonitridophosphates, namely  $\text{Li}_x\text{H}_{12-x-y+z}[\text{P}_{12}\text{O}_{y-24-y}\text{N}_{24-y}]X$  with  $X = \text{Cl}, \text{Br}$ .<sup>[140,141]</sup> The framework is built up from exclusively vertex-sharing *dreier* rings. In case of  $\text{Ba}_3\text{Si}_3\text{N}_5\text{OCl}$  and  $\text{Ba}_6\text{Si}_6\text{N}_{10}\text{O}_2(\text{CN}_2)$ , the large

**Table 1:** Framework density of known zeolites compared to zeolite analogous (oxo)nitridosilicates.<sup>[a]</sup>

Compound	[SiO <sub>4</sub> ]	[SiN <sub>4</sub> ]
Zeolite beta	15.1	(12.1)
Faujasite	12.7	(10.2)
Ba <sub>3</sub> Si <sub>5</sub> N <sub>5</sub> OCl	(16.3)	13.6
Ba <sub>6</sub> Si <sub>10</sub> O <sub>2</sub> (CN <sub>2</sub> )	(17.3)	14.4
Li <sub>2</sub> O@[SrSiN <sub>2</sub> ] <sub>4</sub>	(20.0)	16.7
Ba <sub>2</sub> Nd <sub>7</sub> Si <sub>11</sub> N <sub>23</sub>	(22.2)	18.5
RE <sub>7</sub> Si <sub>6</sub> N <sub>15</sub> (RE = La, Ce, Pr)	(18.2)	15.2
Ba <sub>4</sub> RE <sub>7</sub> [Si <sub>12</sub> N <sub>23</sub> O][BN <sub>3</sub> ] (RE = Pr-Sm)	(20)	17

[a] Numbers in parentheses are fictive values, assuming a 20% higher volume for [SiN<sub>4</sub>] tetrahedra compared to [SiO<sub>4</sub>] tetrahedra.

*zwölfer* ring channels of the *NPO* zeolite structure type are built up from [Si(N/O)<sub>4</sub>] tetrahedra, filled with Ba<sup>2+</sup> ions surrounding strands of Cl<sup>-</sup>/[CN<sub>2</sub>]<sup>2-</sup> ions, respectively (Figure 23 a).

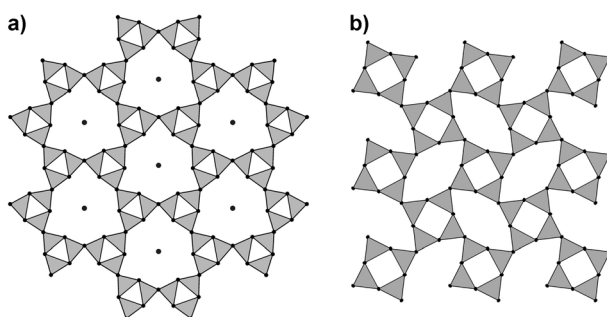


**Figure 23.** a) Structure of Ba<sub>3</sub>Si<sub>5</sub>N<sub>5</sub>OCl and Ba<sub>6</sub>Si<sub>10</sub>N<sub>10</sub>O<sub>2</sub>(CN<sub>2</sub>) with Ba atoms omitted, viewed along [001]. Cl<sup>-</sup> and CN<sub>2</sub><sup>2-</sup> ions are located in the middle of the *zwölfer* ring channels surrounded by Ba<sup>2+</sup> ions. b) [SiN<sub>4</sub>] framework of Li<sub>2</sub>O@[SrSiN<sub>2</sub>]<sub>4</sub> viewed along [001].

The stacking of layers exclusively made up of *vierer* rings leads to the *BCT* zeolite structure type, which is the first framework type observed for both oxo- and nitridosilicates. It exhibits *vierer* rings and *achter* rings along [001] and *sechser* rings along [100]. The nitridosilicate oxide Li<sub>2</sub>Sr<sub>4</sub>Si<sub>4</sub>N<sub>8</sub>O adopts the *BCT* framework type. It can be formulated as Li<sub>2</sub>O@[SrSiN<sub>2</sub>]<sub>4</sub>, as oxide ions together with the Li<sup>+</sup> ions are located in the *vierer* ring channels running along [001] (Figure 23 b). In contrast to classical *BCT*-type oxosilicates, the *achter* ring channels of Li<sub>2</sub>O@[SrSiN<sub>2</sub>]<sub>4</sub> are distorted and filled with Sr<sup>2+</sup> ions. Owing to their distortion, the layers resemble those of the layered silicate apophyllite.<sup>[11]</sup> Accordingly, the framework of Li<sub>2</sub>O@[SrSiN<sub>2</sub>]<sub>4</sub> could also be described by condensation of apophyllite-like layers along [001]. The compound Ba<sub>2</sub>Nd<sub>7</sub>Si<sub>11</sub>N<sub>23</sub> (Figure 24 a) was the first example of a nitridosilicate with a framework density in the range of classical zeolites (FD = 18.5; see Table 1) obtained by a RF-furnace synthesis.<sup>[142]</sup> The structure is made up from bridging N<sup>[2]</sup> and nitrogen atoms, which are terminally bound to Si (N<sup>[1]</sup>), according to  $^3\infty[\text{Si}^{[4]}_{11}\text{N}^{[1]}_{21}\text{N}^{[2]}_{21}]^{25-}$ . With a molar ratio of Si:N = 11:23, the degree of condensation is slightly smaller than in typical oxidic zeolites ((Al,Si):O = 1:2).

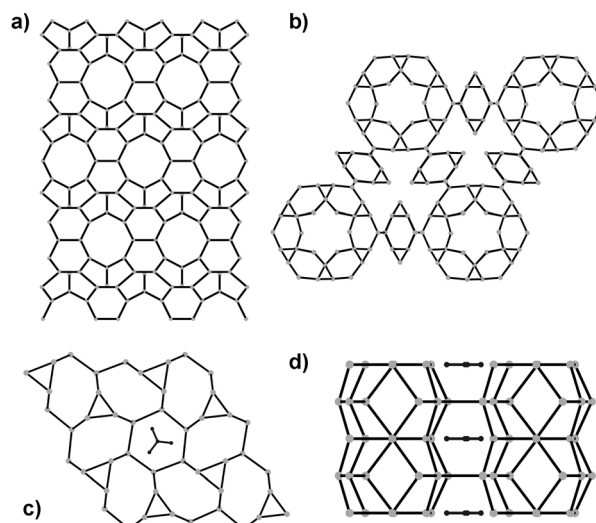


**Figure 24.** a,b) Representations of the zeolite-analogous framework of a) Ba<sub>2</sub>Nd<sub>7</sub>Si<sub>11</sub>N<sub>23</sub> along [001] and b) RE<sub>7</sub>Si<sub>6</sub>N<sub>15</sub> (RE = La, Ce, Pr), viewed along [100], O and N atoms are omitted, and neighboring Si centers (gray) are directly connected. c,d) In the framework of Ba<sub>4</sub>RE<sub>7</sub>[Si<sub>12</sub>N<sub>23</sub>O][BN<sub>3</sub>] with RE = Pr—Sm viewed along c) [001] and d) along [100], isolated [BN<sub>3</sub>]<sup>6-</sup> ions (black) are incorporated.

Characteristic for the unprecedented structure of Ba<sub>2</sub>Nd<sub>7</sub>Si<sub>11</sub>N<sub>23</sub> are *sechser* rings and *achter* rings along [001]. The Ba<sup>2+</sup> ions are centered in the large *achter* rings and the Nd<sup>3+</sup> in the smaller voids. For the nitridosilicates M<sub>7</sub>Si<sub>6</sub>N<sub>15</sub> with M = La, Ce, and Pr, a new structure type with an interrupted framework has been identified (Figure 24 b).<sup>[143]</sup> It is built up exclusively of corner-sharing tetrahedra that appear as Q<sup>2-</sup>, Q<sup>3-</sup>, and Q<sup>4-</sup> type forming a variety of different ring sizes within a less condensed three-dimensional network.

The isotropic compounds Ba<sub>4</sub>RE<sub>7</sub>[Si<sub>12</sub>N<sub>23</sub>O][BN<sub>3</sub>] (RE = Pr-Sm) are made up from orthonitridoborate ions [BN<sub>3</sub>]<sup>6-</sup> encapsulated in oxonitridosilicate cages.<sup>[136]</sup> Therefore, the structure could also be classified as a clathrate, whereas nitridic clathrates are very rare in the literature, the only other known example being P<sub>4</sub>N<sub>4</sub>(NH)<sub>4</sub>(NH<sub>3</sub>).<sup>[144]</sup> From a topological point of view, the framework of Ba<sub>4</sub>RE<sub>7</sub>[Si<sub>12</sub>N<sub>23</sub>O][BN<sub>3</sub>] is composed of exclusively vertex-sharing tetrahedra, exhibiting all possible ring sizes Si<sub>n</sub>(O,N)<sub>n</sub> except n = 2, 4, and 5 (Figure 24 c,d). The [BN<sub>3</sub>]<sup>6-</sup> ions are stacked together with rare earth ions in the *sechser* ring channels along [001]. With respect to a rational planning of the synthesis of zeolite-like (oxo)nitridosilicates, it was assumed that the [BN<sub>3</sub>]<sup>6-</sup> units, like the carbodiimide ions in Ba<sub>6</sub>Si<sub>10</sub>O<sub>2</sub>(CN<sub>2</sub>),<sup>[29]</sup> do not condense with the nitridosilicate framework but act as high-temperature-stable templates around which the framework is organized.

## 6. Chemical Bonding in Nitridosilicates

### 6.1. Bond Lengths and Degree of Condensation

A closer look at the [SiN<sub>4</sub>] tetrahedra in nitridosilicates reveals a broad range for Si–N bond lengths and N–Si–N

angles. The values are strongly dependent on the connection mode of the tetrahedra (for example, vertex- or edge-sharing). Furthermore, the differing connectivity modes of the nitrogen atoms ( $N^{[1]}$ ,  $N^{[2]}$ ,  $N^{[3]}$  and  $N^{[4]}$ ) are responsible for flexible Si–N bond lengths, which range from 164 to 196 pm. In Figure 25, typical ranges of Si–N bond lengths of exem-

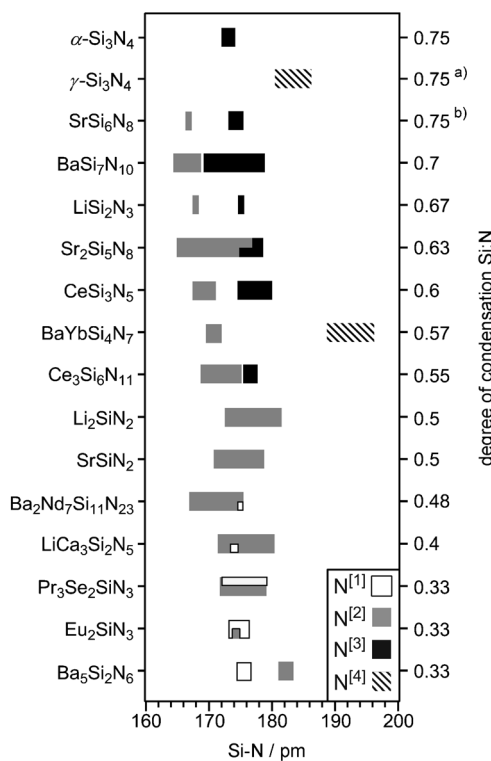


**Figure 25.** Si–N bond lengths in nitridosilicates. The degree of condensation and the molar ratio Si:N increases from bottom to top.  
a) The  $N^{[4]}$  atoms in  $\gamma\text{-Si}_3\text{N}_4$  are part of octahedral  $[\text{SiN}_6]$  units.  
b)  $\text{SrSi}_6\text{N}_8$  has additional Si–Si bonds.

plary nitridosilicates are displayed, considering the respective coordination numbers of the nitrogen atoms. It may be noted that a direct relation between bond lengths and bond strengths in nitridosilicates does not allow for the appraisement of the stability of a compound.  $\text{BaYbSi}_4\text{N}_7$  (Si–N $^{[4]}$  189–196 pm), for example, exhibits a thermal stability up to 1700 °C.<sup>[104]</sup> Calculation of the mean Si $^{[4]}$ –N bond length for the majority of nitridosilicates reported to date results in a value of approximately 174 pm. In comparison to oxosilicates, Liebau reported an average bond length of 162 pm for Si $^{[4]}$ –O.<sup>[1]</sup> These differences in bond lengths allow for the assignment of O/N in ordered oxonitridosilicates, such as  $\text{CaSi}_2\text{O}_2\text{N}_2$  (Si–O: 159–162 pm and Si–N: 168–178 pm). The Si–N–Si angles show a larger flexibility compared to the corresponding values for Si–O–Si in oxosilicates,<sup>[1]</sup> as they range from 82° in  $\text{Ca}_7[\text{NbSi}_2\text{N}_6]$  (owing to edge sharing)<sup>[43]</sup> to up to 180° in  $\text{Ba}_2\text{Nd}_7\text{Si}_{11}\text{N}_{23}$ <sup>[142]</sup> or  $\text{La}_{16}[\text{Si}_8\text{N}_{22}][\text{SiON}_3]_2$  (crosslinking of  $[\text{Si}_2\text{N}_6]_{10}$  units by one N).<sup>[41]</sup>

In Figure 25, the nitridosilicates are ordered by their formal degree of condensation ranging from 0.75 for  $\text{Si}_3\text{N}_4$  to 0.33 for 1D nitridosilicates. The latter value is also found in

structural elements such as isolated  $[\text{Si}_2\text{N}_6]^{10-}$  double tetrahedra, unbranched single chains, and isolated *dreier* rings. A degree of condensation of 0.25 as found in non-condensed orthosilicates has not been structurally verified for nitridosilicates as yet, but has been reported for oxonitridosilicates. The occurrence of Si–Si bonds in the reduced nitridosilicate  $\text{SrSi}_6\text{N}_8$  leads to a higher formal degree of condensation as would be expected for a classical nitridosilicate exhibiting alternating Si and N atoms.<sup>[111]</sup>

## 6.2. Lattice-Energy Calculations According to the MAPLE Concept

Electrostatic lattice energy calculation with the algorithm MAPLE (Madelung part of lattice energy)<sup>[145–147]</sup> is an appropriate method to check crystal structures with respect to their electrostatic plausibility. For each atom, a partial MAPLE value is computed, which lies within a characteristic (empirical) range for each species. These computations exclusively consider electrostatic interactions in ionic crystals and depend on the distance, charge, and coordination of the constituent atoms. Therefore, this method could be especially useful to assign elements to certain sites, which are difficult to distinguish with X-ray methods (for example, O/N or Al/Si, respectively). To determine the total MAPLE value of a compound, the partial MAPLE values for all atoms can be summed up. Furthermore, MAPLE values are additive with high accuracy, allowing for a comparison between the sum of the MAPLE values of the starting materials with the total MAPLE value of the product to check the electrostatic consistency. It should be noted that this algorithm was designed to evaluate more ionic structures (for example oxosilicates); nevertheless, the transfer to the more covalent nitridosilicates still allows for exact calculations. Table 2 compares the partial MAPLE values of  $\text{Eu}_2\text{SiN}_3$  (calculated regarding the crystal structure) with adequate starting materials (summed up to  $\text{Eu}_2\text{SiN}_3$ ).<sup>[47]</sup> In this case, the small difference of 0.4% even includes the correct assignment of the mixed-valent europium sites ( $\text{Eu}^{2+}/\text{Eu}^{3+}$ ).

**Table 2:** MAPLE calculations for  $\text{Eu}_2\text{SiN}_3$ .<sup>[a]</sup>

$\text{Eu}_2\text{SiN}_3$	
Sum of partial MAPLE values	31146
Sum of MAPLE values of starting materials	31270
$\text{EuN} + 1/2 \text{Eu}_2\text{Si}_5\text{N}_8 - 1/2 \text{Si}_3\text{N}_4$	
Difference	0.4%

[a] Values are given in  $\text{kJ mol}^{-1}$ .

As mentioned above, the partial MAPLE values for each ion species exhibit a characteristic range, which was determined by comparing the partial MAPLE values of the same ionic species in different but well-defined nitridosilicates. Table 3 compares the partial MAPLE values for the most common ions observed in nitridosilicates to date; however, these values should be regarded as tendencies, as these ranges

**Table 3:** Typical partial MAPLE values in nitridosilicates.<sup>[a]</sup>

Ion	Typical partial MAPLE values
Si <sup>4+</sup>	9000–10200
Al <sup>3+</sup>	5500–6000
(N <sup>[1]</sup> ) <sup>3-</sup>	4300–5000
(N <sup>[2]</sup> ) <sup>3-</sup>	4600–6000
(N <sup>[3]</sup> ) <sup>3-</sup>	5000–6200
(O <sup>[1]</sup> ) <sup>2-</sup>	2000–2800
(O <sup>[2]</sup> ) <sup>2-</sup>	2400–2800
Ca <sup>2+</sup>	1700–2200
Sr <sup>2+</sup>	1500–2100
Ba <sup>2+</sup>	1500–2000
Eu <sup>2+</sup>	1700–2100
RE <sup>3+</sup>	3500–5100

[a] Values are given in  $\text{kJ mol}^{-1}$ .

are empirically generated.<sup>[148–150]</sup> Nevertheless, a clear tendency of the partial MAPLE values is as follows:  $\text{MAPLE}(\text{N}^{[1]}) \leq \text{MAPLE}(\text{N}^{[2]}) \leq \text{MAPLE}(\text{N}^{[3]}) \leq \text{MAPLE}(\text{N}^{[4]})$ .

## 7. Material Properties

Scientifically, (oxo)nitrido(alumo)silicates are of special interest because their interatomic bonding is likely to cover a wide spectrum from partly ionic, as in the more oxidic representatives, to highly covalent in the nitridic compounds. The prospect of a plethora of hitherto unknown crystal structures seems promising, and elucidation of structure–property relations will be a major goal.

### 7.1. Nitride Ceramics

In the last decades, a variety of investigations on bulk silicon nitride ceramics has been performed because of their physical and mechanical properties, which are of interest for high-temperature applications. These low-density materials exhibit high decomposition temperatures (ca. 1900 °C) combined with high mechanical strength, good thermal shock properties, good oxidation resistance, low coefficient of friction, and good resistance to corrosive environments.<sup>[19,124]</sup> However, limitations occur owing to the poor damage tolerance caused by high sensitivity to flaws or cracks. Therefore, extensive research on microstructural and compositional design has been performed. Important microstructural elements in silicon nitride are elongated matrix grains that are randomly distributed, interlocked, and interspersed with a secondary phase, thus influencing materials characteristics, and particularly the mechanical properties.<sup>[19,151,152]</sup> Therefore, much effort has been directed to understand the formation of these anisotropic grains, as there is a strong dependence on the sintering additives such as rare earth oxides and therefore the dopant cations (for example, Y<sup>3+</sup>, La<sup>3+</sup>, Ce<sup>3+</sup>).<sup>[152–154]</sup> Investigations on doping with oxides led to the discovery of SiAlONs, which are important because of special interest in engineering ceramics and improvement of

fabrication methods by the use of ceramic alloys. Improvements in mechanical strength, oxidation resistance, and creep resistance of hot-pressed silicon nitride required an understanding of oxide–nitride interactions and the formation of oxynitride glasses.<sup>[124]</sup>

Apart from quasi-binary doped silicon nitride/oxide ceramics, bulk nitridosilicates with interesting properties, such as hardness have also been reported. For SrSi<sub>7</sub>N<sub>10</sub> hardness investigations (nanoindentation) exhibit an average Vickers hardness of 16.1(5) GPa ( $E = 115(2)$  GPa),<sup>[103]</sup> which is comparable to values reported for sintered polycrystalline  $\alpha$ -SiAlONs<sup>[155,156] and  $\alpha$ -Al<sub>2</sub>O<sub>3</sub><sup>[157]</sup> (in the range of 21–22 GPa). This high value could be explained by the presence of the 3D network for this structure combined with a very high condensation degree of the [SiN<sub>4</sub>] tetrahedra (see Section 5.1). Very high Vickers hardness values of 22.0 GPa have been measured on single crystals of the SiAlON Sr<sub>3</sub>Pr<sub>10</sub>Si<sub>18</sub>Al<sub>12</sub>O<sub>18</sub>N<sub>36</sub>.<sup>[130]</sup></sup>

### 7.2. Thermal Conductivity

Ceramic materials with high electrical resistivity in combination with high thermal conductivity are potentially interesting as heat sink materials in integrated circuits. As early as 1973, Slack noted that several compounds having an adamantine crystal structure might have a high thermal conductivity (> 100  $\text{W m}^{-1} \text{K}^{-1}$ ).<sup>[158]</sup> AlN in particular has received considerable attention,<sup>[159,160]</sup> but the nitridosilicate materials MgSiN<sub>2</sub> (which can be derived from AlN by replacing 2 Al<sup>3+</sup> by Mg<sup>2+</sup>/Si<sup>4+</sup>)<sup>[161]</sup> and more recently  $\beta$ -Si<sub>3</sub>N<sub>4</sub><sup>[162]</sup> have also been considered to be potentially effective and rather stable thermal conductors. The thermal conductivities estimated by a modified Slack equation for MgSiN<sub>2</sub>, AlN, and  $\beta$ -Si<sub>3</sub>N<sub>4</sub> ceramics at 300 K equal 28, 200, and 105  $\text{W m}^{-1} \text{K}^{-1}$ , respectively, in agreement with the highest experimental values of 25–27, 266, and 105–120  $\text{W m}^{-1} \text{K}^{-1}$ .<sup>[161,163,164]</sup> Further nitridosilicates have been investigated regarding their thermal conductivity. Although smaller values in the range of 3–6  $\text{W m}^{-1} \text{K}^{-1}$  were measured for CaSiN<sub>2</sub>, BaSi<sub>7</sub>N<sub>10</sub>, and M<sub>2</sub>Si<sub>5</sub>N<sub>8</sub> with M = Ca, Sr, Ba, a trend of increasing thermal conductivity with decreasing M/Si ratio might suggest a relationship with the network connectivity.<sup>[165]</sup>

### 7.3. Lithium Ion Conductivity

Syntheses and properties of lithium nitridosilicates have been investigated for some time for targeting applications as efficient ion conductors and nitrogen sensors.<sup>[5,39,166]</sup> The possibility of lithium ions to move effectively through silicon nitride frameworks renders these materials possible candidates for solid-state electrolytes in lithium batteries.<sup>[167]</sup> As mentioned above (Section 3), several lithium nitridosilicates have been reported (for example LiSi<sub>2</sub>N<sub>3</sub>,<sup>[36,37]</sup> Li<sub>2</sub>SiN<sub>2</sub>,<sup>[37–39]</sup> Li<sub>5</sub>SiN<sub>3</sub>,<sup>[5,40]</sup> Li<sub>8</sub>SiN<sub>4</sub>,<sup>[37,39]</sup> Li<sub>18</sub>Si<sub>3</sub>N<sub>10</sub>, and Li<sub>21</sub>Si<sub>3</sub>N<sub>11</sub>).<sup>[39]</sup> Lithium ion conductivity has been observed and comprehensively studied for Li<sub>2</sub>SiN<sub>2</sub> ( $\sigma(400 \text{ K}) = 1.1 \times 10^{-3} \Omega^{-1} \text{cm}^{-1}$ ) and

$\text{Li}_8\text{SiN}_4$  ( $\sigma(400 \text{ K}) = 5 \times 10^{-2} \Omega^{-1} \text{cm}^{-1}$ ).<sup>[37,81,168]</sup> The orthosilicate-type  $[\text{SiN}_4]^{8-}$  tetrahedra and also the high lithium content might favor the high lithium conductivity of  $\text{Li}_8\text{SiN}_4$ .<sup>[37,39]</sup> Recent structural elucidation of  $\text{Li}_2\text{SiN}_2$  revealed the existence of short Li–Li contacts and edge/face sharing of  $[\text{LiN}_x]$  polyhedra, allowing an assumption of possible lithium pathways for  $\text{Li}^+$  ion conductivity.<sup>[38]</sup> According to this assumption, the  $\text{Li}^+$  ions could move in layers parallel to [001] (Figure 26). Nevertheless,  $\text{Li}^+$  ion conductivity results from complex interactions of structural features, defects, and vacancies, and cannot usually be explained exclusively by structural arguments.

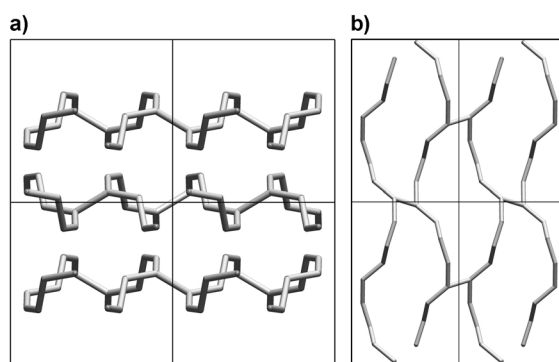


**Figure 26.** Illustration of possible channels constructed by short Li–Li distances viewed along a) [001] and b) [010]. The  $\text{Li}^+$  ions are connected by bonds (shown in dark gray) forming layers parallel to [001].<sup>[38]</sup>

Recently, a novel synthetic approach to lithium nitridosilicates involving the use of lithium melts has been described.<sup>[28]</sup> This led to the discovery of novel compounds which might represent some promising lithium ion conduction materials (for example,  $\text{Li}_4\text{M}_3\text{Si}_2\text{N}_6$  with  $\text{M} = \text{Ca}, \text{Sr}$ ,<sup>[28,44]</sup>  $\text{LiCa}_3\text{Si}_2\text{N}_5$ ,<sup>[28]</sup>  $\text{Li}_5\text{RE}_5\text{Si}_4\text{N}_{12}$  ( $\text{RE} = \text{La}, \text{Ce}$ )<sup>[46]</sup>  $\text{Li}_2\text{MSi}_2\text{N}_4$  with  $\text{M} = \text{Ca}, \text{Sr}$ <sup>[85]</sup> and  $\text{Li}_2\text{Sr}_4\text{Si}_4\text{N}_8\text{O}$ <sup>[28]</sup>).

#### 7.4. Nonlinear Optical (NLO) Materials

During the last decades, a growing interest has emerged in the field of nonlinear optical (NLO) phenomena (for example, SHG) and development of nonlinear optical materials that possess commercial device applicability. These materials can be utilized in computer and optical signal processing devices (for example, optical switching, optical data processing),<sup>[169,170]</sup> optical frequency conversion, and telecommunications. With the advancing development of optotechnologies, new materials with high nonlinear optical susceptibilities and high damage thresholds are of particular interest. Transparent and colorless materials with non-centrosymmetric crystal structures, such as alkaline earth nitridosilicates with their superior mechanical properties and their extraordinary chemical and thermal stability, are attractive candidates for this purpose. However, nonlinear optical properties of nitridosilicates have been scarcely investigated.<sup>[171]</sup> Owing to the present unavailability of large

nitridosilicate single crystals, other powder-based techniques have been used to study the nonlinear susceptibility  $\chi^{(2)}$ , namely the Kurtz–Perry method<sup>[172]</sup> and the SHEW method (second harmonic wave generated by an evanescent wave).<sup>[173,174]</sup> These SHEW investigations have revealed high refractive indices for  $\text{M}_2\text{Si}_3\text{N}_8$  with  $\text{M} = \text{Ca}, \text{Sr}$  with values between 2 and 3. The averaged effective Figure of Merit  $M_{\text{eff}} = (d_{\text{eff}}^2)/(n_{2\omega} n_{\omega}^2)$  with  $d_{\text{eff}} = 0.5 \chi_{\text{eff}}^{(2)}$  (a measure for the efficiency of the nonlinear interaction process) was found to be of the same order of magnitude as that of  $\text{LiIO}_3$  in the most efficient samples (see Table 4).<sup>[171,175]</sup> These values are a promising starting point for further single-crystal investigations on nitridosilicate materials; however, crystal-growth techniques for large nitridosilicate samples appear to be scarce.

**Table 4:** Averaged figure of merit  $M_{\text{eff}}$ .<sup>[a]</sup>

Sample	$n_{\omega}$	$n_{2\omega}$	$M_{\text{eff}} [\text{pm}^2 \text{V}^{-2}]$ Kurtz–Perry	$M_{\text{eff}} [\text{pm}^2 \text{V}^{-2}]$ SHEW
$\text{LiIO}_3$	1.72	1.90	1.6	1.6
$\text{Ba}_2\text{Si}_5\text{N}_8$	—	—	—	—
$\text{Sr}_2\text{Si}_5\text{N}_8$	2.5	2.6	0.2	0.8
$\text{Ca}_2\text{Si}_5\text{N}_8$	2.55	2.65	0.04	0.9
$\text{BaYbSi}_4\text{N}_7$	—	—	0.02	—
$\text{CeSi}_3\text{N}_5$	—	—	0.4	—
KDP <sup>[b]</sup>	1.49	1.51	0.02	—

[a]  $M_{\text{eff}} = (d_{\text{eff}}^2)/(n_{2\omega} n_{\omega}^2)$  determined by the Kurtz–Perry and SHEW methods.<sup>[171]</sup> [b] KDP =  $\text{KH}_2\text{PO}_4$ .

Furthermore, interesting two-photon absorption processes have been investigated in  $\text{Eu}_2\text{Si}_3\text{N}_8$  upon irradiation with an infrared laser ( $\lambda = 1047 \text{ nm}$ ) resulting in red fluorescence emission.<sup>[175]</sup> Besides promising luminescence properties upon doping (see Section 7.5),  $\text{Ba}_2\text{Si}_5\text{N}_8:\text{Eu}^{2+}$  also exhibits a relatively strong two-photon absorption, which can be used for upconversion purposes. If this material is excited with intense ultrashort pulses from a Nd:YLF laser (wavelength  $1.047 \mu\text{m}$ , 7 ps duration), a fluorescence emission at about 600 nm is generated, which amounts to roughly  $10^{-7}$  of the fluorescence emission after excitation at 523 nm by a frequency-doubled laser.<sup>[176]</sup> Achieving such an efficiency with a relatively low excitation intensity of about  $1 \text{ MW/cm}^2$  is an indication of a fairly high two-photon absorption cross-section.

#### 7.5. Luminescence

An exciting new field of research for (oxo)nitrido-(alumo)silicates, the use as a novel class of inorganic phosphors, has emerged in the last few years. With the technological access to p-doped GaN,<sup>[177]</sup> Nakamura opened the path to a formidable development of efficient blue LEDs. This improvement leads to the need for suitable luminescent materials (phosphors) to generate white light, which is usually achieved by 1) using three individual monochromatic LEDs (blue, green, red); 2) combining an ultraviolet LED with blue, green, and red phosphors; or 3) using a blue LED to pump

yellow or green and red phosphors.<sup>[94]</sup> To this end, in the latter two cases in particular, appropriate phosphors as down-conversion luminescent materials for phosphor-converted (pc)-LEDs are needed. These phosphors should match a series of requirements, starting with the efficient absorption of UV or blue light, which is generated from the primary LED. Further characteristics, such as high conversion efficiency and high chemical and thermal stability, are necessary requirements for these materials. During the last several years, the discovery and development of new phosphors moved the field of LED phosphors from a single family of phosphor compositions, the Ce<sup>3+</sup>-doped YAG (i.e. yttrium aluminum garnet), to a plethora of compounds, such as orthosilicates,<sup>[178–180]</sup> aluminates,<sup>[180]</sup> sulfides,<sup>[180,181]</sup> and fluorides<sup>[182,183]</sup> predominantly doped with Ce<sup>3+</sup> or Eu<sup>2+</sup>. Nevertheless, some of these phosphors exhibit the problem of low absorption in the visible-light spectrum or high thermal quenching. Sulfide-based phosphors in particular suffer from thermal and moisture sensitivity, requiring effective coating of the phosphor grains in pc-LEDs.

The class of Eu<sup>2+</sup>-doped (oxo)nitridosilicates emerged as extraordinarily efficient materials that are applicable in pc-LEDs owing to their high chemical and thermal stability in combination with low thermal quenching and high conversion efficiencies.<sup>[93,94,184]</sup> Furthermore, the energy position of the Eu<sup>2+</sup>/Ce<sup>3+</sup> 4f<sup>N</sup>-5d<sup>1</sup> level and the 4f<sup>N</sup>→4f<sup>N-1</sup>5d<sup>1</sup> transitions in inorganic hosts is modified by the covalency and polarizability of Eu<sup>2+</sup>/Ce<sup>3+</sup>-ligand bonds.<sup>[185–187]</sup> In (oxo)nitridosilicates, the activator is surrounded by a network of predominantly [SiN<sub>4</sub>] tetrahedra. Therefore, the more polarizable nitridic surroundings lower the excited state of the 5d electrons of doped rare earth elements owing to large crystal-field splitting and a strong nephelauxetic effect compared to oxidic surroundings. This can shift the excitation and emission bands to larger wavelengths because it reduces the energy difference between the ground state and the excited state of rare earth ions. Furthermore, the structural versatility of (oxo)nitridosilicate phosphor materials allows generation of emission colors across the entire visible spectrum from blue to red, and especially in wavelength ranges in which direct radiation from non-converted LEDs is relatively inefficient, that is, in the so-called “yellow gap”.<sup>[89]</sup>

Today, there are several rare earth-doped (oxo)nitridosilicate compounds that exhibit interesting luminescence properties. This review will give a brief overview on some of the most promising phosphors; more extensive reviews on luminescence of (oxo)nitridosilicates have recently been published by Höpke,<sup>[188]</sup> Xie,<sup>[94]</sup> Setlur,<sup>[189]</sup> He,<sup>[190]</sup> and others.

In 1997, Huppertz was the first to report the deep-red luminescence of Eu<sub>2</sub>Si<sub>5</sub>N<sub>8</sub> upon excitation with UV light (Figure 27).<sup>[175]</sup>

One year later, van Krevel et al. reported new phosphors doped with Ce<sup>3+</sup>, for example Y<sub>5</sub>(SiO<sub>4</sub>)<sub>3</sub>N, Y<sub>4</sub>Si<sub>2</sub>O<sub>7</sub>N<sub>2</sub>, YSiO<sub>2</sub>N, and Y<sub>2</sub>Si<sub>3</sub>O<sub>3</sub>N<sub>4</sub>,<sup>[191]</sup> followed by the doping of M<sub>2</sub>Si<sub>5</sub>N<sub>8</sub> (M=Ca, Sr, Ba) with Eu<sup>2+</sup> reported by Höpke et al.<sup>[176]</sup> and van Krevel.<sup>[192]</sup> Since then, many investigations on the 2-5-8 family and solid solutions thereof have been performed regarding luminescence and material properties.<sup>[23,34,35,193]</sup> These compounds are very useful for pc-



Figure 27. An image of Eu<sub>2</sub>Si<sub>5</sub>N<sub>8</sub> irradiated under UV light.<sup>[175]</sup>

LEDs, as apart from remarkable optical properties they allow for a tailor-made tuning of the emission wavelength through chemical control of the solid-solution series.<sup>[194,195]</sup> Furthermore, this phosphor class has already found industrial applications in high-power full conversion and warm white LEDs.<sup>[93]</sup> Highly efficient monochromatic pc-LEDs with very good performance and a color purity of more than 96 % have been developed using a Lumiramic version of a 2-5-8 phosphor (see Figure 28) with inherently good thermal and drive stability when matched with a high performance TFFC-LED.<sup>[15,89,196]</sup>

ue mentioned in general  
olved, even with employ  
lab result at present sho  
s the birefringence of th  
rays cause some scatterin  
sons have not been com  
ements of the lumen outp

Figure 28. Translucent Lumiramic wafer made up from Eu<sup>2+</sup>-doped M<sub>2</sub>Si<sub>5</sub>N<sub>8</sub> (photograph courtesy of Philips Research).

Doping with Eu<sup>2+</sup> of oxonitridosilicates of formula type MSi<sub>2</sub>O<sub>2</sub>N<sub>2</sub> with M=Ca, Sr, Ba (so called 1-2-2-2 materials) came out as a very efficient and promising class of phosphors. The emission varies over a wide range from about 498 nm (BaSi<sub>2</sub>O<sub>2</sub>N<sub>2</sub>:Eu<sup>2+</sup>) over about 540 nm (SrSi<sub>2</sub>O<sub>2</sub>N<sub>2</sub>:Eu<sup>2+</sup>), to about 560 nm (CaSi<sub>2</sub>O<sub>2</sub>N<sub>2</sub>:Eu<sup>2+</sup>).<sup>[197,198]</sup> Again, the availability of solid-solution series allows for a color point tuning and application for white-light LEDs.<sup>[64]</sup> Furthermore, the luminescence intensity of SrSi<sub>2</sub>O<sub>2</sub>N<sub>2</sub>:Eu<sup>2+</sup> can be remarkably enhanced by co-doping with Ce<sup>3+</sup>, Dy<sup>3+</sup>, and Mn<sup>2+</sup>.<sup>[199]</sup> In 2005, Müller-Mach et al. reported an unprecedented, highly efficient all-nitride phosphor-converted warm-white-light LED comprising Eu<sup>2+</sup>-doped 2-5-8 (orange-red) and 1-2-2-2 (yellow-green) phosphor excited by a GaN-based quantum-well blue LED (see Figure 29).<sup>[93]</sup>

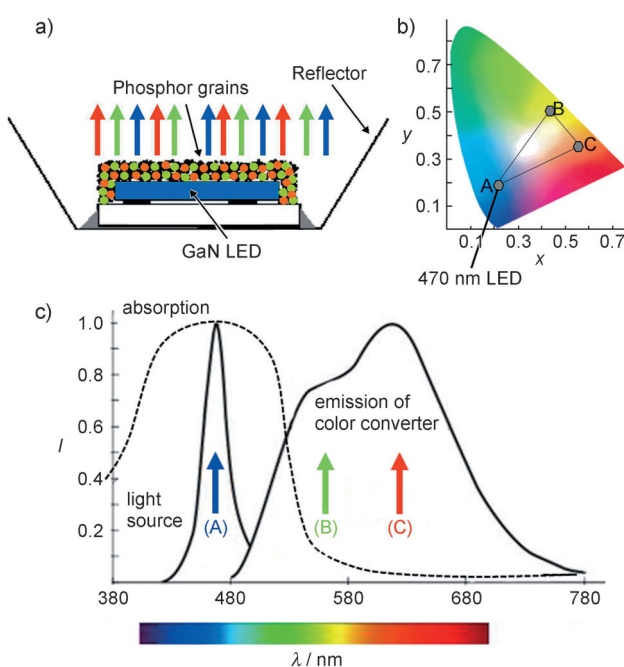


**Figure 29.** a) Illustration of a two phosphor-converted LED. b) CIE color diagram (CIE = Commission Internationale d'Eclairage); by mixing the three emissions A, B, and C defined by their color coordinates, all colors within the triangle are accessible by additive color mixing. c) Absorption and emission spectra of a two phosphor-converted LED. A: GaN, B:  $\text{SrSi}_2\text{O}_2\text{N}_2:\text{Eu}^{2+}$ , C:  $\text{Sr}_2\text{Si}_5\text{N}_8:\text{Eu}^{2+}$ .

$\text{CaAlSiN}_3:\text{Eu}^{2+}$  (CASN), a very promising phosphor with emission in the red spectral region ( $\lambda_{\text{max}} \approx 650 \text{ nm}$ ) and QEs > 85% beyond 200°C, was synthesized and characterized by Uheda et al.<sup>[184]</sup> Especially interesting is the synthesis of the solid-solution series  $(\text{Ca}_{1-x}\text{Sr}_x\text{AlSiN}_3:\text{Eu}^{2+})$  and the complete exchange of Ca by Sr as the emission maximum can thus be tuned down to 610 nm.<sup>[200]</sup> However, high-pressure nitridation synthesis (pressure up to 190 MPa) was necessary to yield the metastable  $\text{Ca}_{1-x}\text{Sr}_x\text{AlSiN}_3:\text{Eu}^{2+}$  compounds.<sup>[201]</sup>

In recent years, RE-activated  $\alpha$ -SiAlON luminescent materials (especially  $\text{Eu}^{2+}$ -activated) have attracted much attention because the photoluminescence properties can be influenced by controlling the overall composition of the  $\alpha$ -SiAlON host lattice or by altering the  $\text{Eu}^{2+}$  doping concentration.<sup>[202–204]</sup> Intensive research has been performed on  $\text{Eu}^{2+}$ -doped Ca- $\alpha$ -SiAlON, which shows a single intense broadband emission at 583–603 nm,<sup>[205]</sup> and Li- $\alpha$ -SiAlON, in which emission can be tuned across a wide range of 563–586 nm by tailoring the Al/Si or O/N ratios of the host lattice or by controlling the  $\text{Eu}^{2+}$  concentration.<sup>[206]</sup> Hirosaki et al. reported the  $\text{Eu}^{2+}$ -activated  $\beta$ -SiAlON green-emitting phosphor, which peaked at 528–550 nm and exhibits low thermal quenching and a high stability of chromaticity against temperature.<sup>[207,208]</sup>

Much effort has been directed to discover novel phosphor compounds by intensive investigations of (oxo)nitrido-(alumo)silicate compositional phase diagram spaces. This has led to recent discoveries of interesting luminescent materials, such as yellow  $\text{Ba}_2\text{AlSi}_5\text{N}_9:\text{Eu}^{2+}$ <sup>[117]</sup> and orange-red  $\text{SrAlSi}_4\text{N}_7:\text{Eu}^{2+}$ <sup>[116]</sup> as well as green

$\text{Sr}_5\text{Al}_{5+x}\text{Si}_{21-x}\text{N}_{35-x}\text{O}_{2+x}:\text{Eu}^{2+}$  (with  $x \approx 0$ )<sup>[132]</sup> and green  $\text{Ba}_3\text{Si}_6\text{O}_{12}\text{N}_2:\text{Eu}^{2+}$ .<sup>[67,209]</sup>

Recently, growing interest in first-principles electronic structure calculations of nitridosilicates has emerged.<sup>[210–212]</sup> In particular, band-gap and bonding-character calculations are important to gain more knowledge about electronic transitions. However, band structure calculations appear to be very complex; for example, the band gap of  $\text{Ba}_3\text{Si}_6\text{O}_{12}\text{N}_2$  was computed to be 4.63 eV,<sup>[209]</sup> whereas recent investigations calculated a band gap of 6.93 eV using the mBJ-GGA potential.<sup>[67]</sup> Furthermore, the band gap of  $\text{Ba}_3\text{Si}_6\text{O}_{12}\text{N}_2:\text{Eu}^{2+}$  was measured to be  $(7.05 \pm 0.25)$  eV by means of X-ray emission spectroscopy (XES) and X-ray absorption near-edge spectroscopy (XANES).<sup>[67]</sup> In any case, there is a need for more progress in the field of first-principles electronic structure calculations to obtain reliable information of the band gap and perhaps, in near future, of electronic transitions involving the excited states of phosphor materials.

The class of (oxo)nitrido(alumo)silicate phosphors has demonstrated its superior suitability for use in white pc-LEDs owing to excellent properties of high luminous efficacy, high chromatic stability, a wide range of white light with adjustable correlated color temperatures (CCTs), and brilliant color-rendering properties in conjunction with a wide structural diversity, leaving space for the discovery of further interesting materials with promising luminescence properties.

## 8. Outlook

Historically, investigation of nitridosilicates and related compounds was primarily driven by purely scientific curiosity. Synthetic challenges have been mastered by the development of new high-temperature reactions, employment of liquid alkali metals as non-conventional solvents, precursor approaches, or carbothermal reduction and nitridation processes starting from the respective oxides. Subsequently, a whole new realm of nitridosilicates, oxonitridosilicates, and SiAlONs with manifold structures and a remarkably broad range of material properties have become available. However, compared to the large and multifarious world of classical oxosilicates, the number of nitridosilicates and related compounds is still small. Nevertheless, a fascinating diversity has been found in this class of compounds, surpassing the structural variability (connectivity and cross-linking modes) of oxosilicates significantly. From a systematic point of view, oxosilicates as well as nitridosilicates, oxonitridosilicates or nitridoalumosilicates, are only subsets of the even more varied superordinate class of oxonitridoalumosilicates (SiAlONs).

Similar to silicon nitride, a number of nitridosilicates and related compounds exhibit high thermal, chemical, and mechanical stability, a high band gap, and a substantial index of refraction. The crystal structures of highly condensed nitridosilicates indicate a significant cumulation of non-centrosymmetric space groups. Accordingly, applications based on nonlinear phenomena (for example, second-harmonic generation (SHG), two-photon absorption) seem to be promising for this class of compounds. In this respect,

significant advancement in crystal growth would be highly desirable. Ammonothermal approaches in supercritical NH<sub>3</sub> could possibly clear the way to large and optically immaculate single crystals of these refractory nitridic materials. Extraordinary potential for further scientific development seems to exist on the field of rare earth-doped non-metal nitrides, some of them being extremely effective luminescent materials for down-conversion applications. Unlike most other substance classes, a number of nitridosilicates and oxonitridosilicates exhibit promising material properties, such as very high chemical and thermal stability, no absorption and high transparency in the visible region of the spectrum, and a large band gap, rendering these materials ideal host compounds for doping with Eu<sup>2+</sup> or Ce<sup>3+</sup>. Such compounds have emerged as highly effective optical functional materials, affording phosphor-converted light-emitting diodes (pc-LEDs) based on high-power primary blue GaN-based LEDs. These devices have the potential to entirely substitute both incandescent and fluorescent lamps, which would lead to dramatic global energy savings.<sup>[15]</sup> Currently, Eu<sup>2+</sup>-doped nitridosilicates, oxonitridosilicates, and related compounds have the highest potential for application as effective luminescent materials in pc-LEDs and they are already being industrially produced.<sup>[89]</sup> Such considerations could be a strong incentive for further exploring the manifold world of nitridosilicates, oxonitridosilicates, and SiAlONs.

*The authors thank Manuel Klein for designing the frontispiece. We would like to thank the German Research Foundation (DFG) and the Fonds der Chemischen Industrie (FCI), Germany, for generous financial support. The authors acknowledge gratefully grants for M.Z. and S.P. by the Dr. Klaus Römer Foundation, Munich.*

Received: September 14, 2010

Published online: July 19, 2011

- [1] F. Liebau, *Structural Chemistry of Silicates*, Springer, Berlin, 1985.
- [2] F. Liebau, *Angew. Chem.* **1999**, *111*, 1845–1850; *Angew. Chem. Int. Ed.* **1999**, *38*, 1733–1737.
- [3] A. Weiss, *Angew. Chem.* **1981**, *93*, 843–854; *Angew. Chem. Int. Ed. Engl.* **1981**, *20*, 850–860.
- [4] M. Lundqvist, P. Nygren, B.-H. Jonsson, K. Broo, *Angew. Chem.* **2006**, *118*, 8349–8353; *Angew. Chem. Int. Ed.* **2006**, *45*, 8169–8173.
- [5] R. Juza, H. H. Weber, E. Meyer-Simon, *Z. Anorg. Allg. Chem.* **1953**, *273*, 48–64.
- [6] H. Lange, G. Wötting, G. Winter, *Angew. Chem.* **1991**, *103*, 1606–1625; *Angew. Chem. Int. Ed. Engl.* **1991**, *30*, 1579–1597.
- [7] W. Schnick, *Angew. Chem.* **1993**, *105*, 846–858; *Angew. Chem. Int. Ed. Engl.* **1993**, *32*, 806–818.
- [8] K. Kim, W. R. L. Lambrecht, B. Segall, *Phys. Rev. B* **1996**, *53*, 16310–16326.
- [9] Y. Oyama, O. Kamigaito, *Jpn. J. Appl. Phys.* **1971**, *10*, 1637.
- [10] K. H. Jack, W. I. Wilson, *Nature phys. Sci.* **1972**, *238*, 28–29.
- [11] W. H. Baur, *Nature* **1972**, *230*, 461–462.
- [12] A. Bischoff, T. Grund, T. Jording, B. Heying, R.-D. Hoffmann, U. Ch. Rodewald, R. Pöttgen, *Z. Naturforsch. B* **2005**, *60b*, 1231–1234.
- [13] W. Schnick, H. Huppertz, *Chem. Eur. J.* **1997**, *3*, 679–683.
- [14] A. Weiss, A. Weiss, *Z. Anorg. Allg. Chem.* **1954**, *276*, 95–112.
- [15] W. Schnick, *Phys. Status Solidi RRL* **2009**, *3*, A113–A114.
- [16] G. Routschka, H. Wuthnow, *Pocket Manual Refractory Materials: Design, Properties and Testing*, Vulkan-Verlag, Essen, 2008.
- [17] M. K. Cinibulk, G. Thomas, *J. Am. Ceram. Soc.* **1992**, *75*, 2050–2055.
- [18] G. N. Babini, A. Bellosi, P. Vincenzini, *J. Am. Ceram. Soc.* **1981**, *64*, 578–584.
- [19] A. Ziegler, J. C. Idrobo, M. K. Cinibulk, C. Kisielowski, N. D. Browning, R. O. Ritchie, *Science* **2004**, *306*, 1768–1770.
- [20] W. Schnick, H. Huppertz, R. Lauterbach, *J. Mater. Chem.* **1999**, *9*, 289–296.
- [21] P. S. Gopalakrishnan, P. S. Lakshminarasimhan, *J. Mater. Sci. Lett.* **1993**, *12*, 1422–1424.
- [22] E. I. Givargizov, *Curr. Top. Mater. Sci.* **1978**, *1*, 79–145.
- [23] X. Piao, T. Horikawa, H. Hanzawa, K. Machida, *Appl. Phys. Lett.* **2006**, *88*, 161908.
- [24] H. Yamane, F. J. DiSalvo, *J. Alloys Compd.* **1996**, *240*, 33–36.
- [25] Z. A. Gál, P. M. Mallinson, H. J. Orchard, S. J. Clarke, *Inorg. Chem.* **2004**, *43*, 3998–4006.
- [26] P. Hubberstey, P. G. Roberts, *J. Chem. Soc. Dalton Trans.* **1994**, 667–673.
- [27] R. J. Pulham, P. Hubberstey, *J. Nucl. Mater.* **1983**, *115*, 239–250.
- [28] S. Pagano, S. Lupart, M. Zeuner, W. Schnick, *Angew. Chem.* **2009**, *121*, 6453–6456; *Angew. Chem. Int. Ed.* **2009**, *48*, 6335–6338.
- [29] S. Pagano, O. Oeckler, T. Schröder, W. Schnick, *Eur. J. Inorg. Chem.* **2009**, 2678–2683.
- [30] T. Hashimoto, F. Wu, M. Saito, K. Fujito, J. S. Speck, S. Nakamura, *J. Cryst. Growth* **2008**, *310*, 876–880.
- [31] D. Peters, *J. Cryst. Growth* **1990**, *104*, 411–418.
- [32] B. Wang, M. J. Callahan, *Cryst. Growth Des.* **2006**, *6*, 1227–1246.
- [33] J. Li, T. Watanabe, N. Sakamoto, H. Wada, T. Setoyama, M. Yoshimura, *Chem. Mater.* **2008**, *20*, 2095–2105.
- [34] M. Zeuner, F. Hintze, W. Schnick, *Chem. Mater.* **2009**, *21*, 336–342.
- [35] M. Zeuner, P. J. Schmidt, W. Schnick, *Chem. Mater.* **2009**, *21*, 2467–2473.
- [36] M. Orth, W. Schnick, *Z. Anorg. Allg. Chem.* **1999**, *625*, 1426–1428.
- [37] J. Lang, J.-P. Charlot, *Rev. Chim. Miner.* **1970**, *7*, 121–131.
- [38] S. Pagano, M. Zeuner, S. Hug, W. Schnick, *Eur. J. Inorg. Chem.* **2009**, 1579–1584.
- [39] H. Yamane, S. Kikkawa, M. Koizumi, *Solid State Ionics* **1987**, *25*, 183–191.
- [40] A. T. Dadd, P. Hubberstey, *J. Chem. Soc. Dalton Trans.* **1982**, 2175–2179.
- [41] C. Schmolke, S. Lupart, W. Schnick, *Solid State Sci.* **2009**, *11*, 305–309.
- [42] H. A. Höppe, G. Kotzyba, R. Pöttgen, W. Schnick, *J. Solid State Chem.* **2002**, *167*, 393–401.
- [43] F. Ottinger, R. Nesper, *Z. Anorg. Allg. Chem.* **2005**, *631*, 1597–1602.
- [44] S. Pagano, S. Lupart, S. Schmiechen, W. Schnick, *Z. Anorg. Allg. Chem.* **2010**, *636*, 1907–1909.
- [45] F. Lissner, T. Schleid, *Z. Anorg. Allg. Chem.* **2004**, *630*, 2226–2230.
- [46] S. Lupart, M. Zeuner, S. Pagano, W. Schnick, *Eur. J. Inorg. Chem.* **2010**, 2636–2641.
- [47] M. Zeuner, S. Pagano, P. Matthes, D. Bichler, D. Johrendt, T. Harmening, R. Pöttgen, W. Schnick, *J. Am. Chem. Soc.* **2009**, *131*, 11242–11248.
- [48] The stretching factor is defined by Liebau as  $f_S = I_{\text{chain}}/(l_T P)$ , with  $I_{\text{chain}}$  being the distance of one period,  $l_T$  the edge length of the tetrahedra, and  $P$  the periodicity of the chain.

- [49] Liebau established the terms *zweier*, *dreier*, *vierer*, *fünfer* chains. A *zweier* chain can be described as two polyhedra within one repeating unit of the linear part of the chain. The terms derive from the German numbers drei, vier, fünf by suffixing “er” to the numeral. F. Liebau, *Structural Chemistry of Silicates*, Springer, Berlin, 1985.
- [50] C. Schmolke, D. Bichler, D. Johrendt, W. Schnick, *Solid State Sci.* **2009**, *11*, 389–394.
- [51] S. Lupart, W. Schnick, *Acta Crystallogr. Sect. E: Struct. Rep. Online* **2009**, *65*, i43.
- [52] O<sup>1</sup>-type [SiN<sub>4</sub>] tetrahedra are connected with one vertex to the next tetrahedron, therefore representing a terminal unit.
- [53] T. Endo, Y. Sato, H. Takizawa, M. Shimada, *J. Mater. Sci. Lett.* **1992**, *11*, 424–426.
- [54] M. Wintenberger, R. Marchand, M. Maunaye, *Solid State Commun.* **1977**, *21*, 733–735.
- [55] P. Eckerlin, Z. Anorg. Allg. Chem. **1967**, *353*, 225–235.
- [56] P. Eckerlin, A. Rabenau, H. Nortmann, Z. Anorg. Allg. Chem. **1967**, *353*, 113–121.
- [57] J. David, Y. Laurent, J. Lang, *Bull. Soc. Fr. Mineral. Cristallogr.* **1970**, *93*, 153–159.
- [58] M. Wintenberger, F. Tcheou, J. David, J. Lang, Z. Naturforsch. **1980**, *35b*, 604–606.
- [59] S. R. Römer, P. Kroll, W. Schnick, *J. Phys.: Condens. Matter* **2009**, *21*, 275408.
- [60] H. A. Höppe, F. Stadler, O. Oeckler, W. Schnick, *Angew. Chem.* **2004**, *116*, 5656–5659; *Angew. Chem. Int. Ed.* **2004**, *43*, 5540–5542.
- [61] O. Oeckler, F. Stadler, T. Rosenthal, W. Schnick, *Solid State Sci.* **2007**, *9*, 205–212.
- [62] F. Stadler, O. Oeckler, H. A. Höppe, M. H. Möller, R. Pöttgen, B. D. Mosel, P. Schmidt, V. Duppel, A. Simon, W. Schnick, *Chem. Eur. J.* **2006**, *12*, 6984–6990.
- [63] J. A. Kechele, O. Oeckler, F. Stadler, W. Schnick, *Solid State Sci.* **2009**, *11*, 537–543.
- [64] V. Bachmann, C. Ronda, O. Oeckler, W. Schnick, A. Meijerink, *Chem. Mater.* **2009**, *21*, 316–325.
- [65] F. Stadler, W. Schnick, Z. Anorg. Allg. Chem. **2006**, *632*, 949–954.
- [66] R. Grün, *Acta Crystallogr. Sect.* **1979**, *35*, 800–804.
- [67] C. Braun, M. Seibald, S. L. Börger, O. Oeckler, T. D. Boyko, A. Moewes, G. Miehe, A. Tücks, W. Schnick, *Chem. Eur. J.* **2010**, *16*, 9646–9657.
- [68] E. Irran, K. Köllisch, S. Leoni, R. Nesper, P. F. Henry, M. T. Weller, W. Schnick, *Chem. Eur. J.* **2000**, *6*, 2714–2720.
- [69] R. Riedel, A. Zerr, G. Miehet, G. Serghiot, M. Schwarz, E. Kroke, H. Fue, P. Kroll, R. Boehler, *Nature* **1999**, *400*, 340–342.
- [70] T. Sekine, H. He, T. Kobayashi, M. Zhang, F. Xu, *Appl. Phys. Lett.* **2000**, *76*, 3706–3708.
- [71] C. M. Fang, G. A. deWijs, H. T. Hintzen, G. deWith, *J. Appl. Phys.* **2003**, *93*, 5175–5180.
- [72] W. Paszkowicz, R. Minikayev, P. Piszora, M. Knapp, C. Bähtz, J. M. Recio, M. Marques, P. Mori-Sánchez, L. Gerward, J. Z. Jiang, *Phys. Rev. B* **2004**, *69*, 052103.
- [73] J. Z. Jiang, H. Lindelov, L. Gerward, K. Stahl, J. M. Recio, P. Mori-Sánchez, S. Carlson, M. Mezouar, E. Dooryhee, A. Fitch, D. J. Frost, *Phys. Rev. B* **2002**, *65*, 161202.
- [74] A. Togo, P. Kroll, *J. Comput. Chem.* **2008**, *29*, 2255–2259.
- [75] D. Peters, H. Jacobs, *J. Less-Common Met.* **1989**, *146*, 241–249.
- [76] H. Völlenkle, *Z. Kristallogr.* **1981**, *154*, 77–81.
- [77] I. Idrestedt, C. Brosset, *Acta Chem. Scand.* **1964**, *18*, 1879–1886.
- [78] H. P. Baldus, W. Schnick, J. Lücke, U. Wannagat, G. Bogedain, *Chem. Mater.* **1993**, *5*, 845–850.
- [79] H. Mengis, H. Jacobs, *Eur. J. Solid State Inorg. Chem.* **1993**, *30*, 45–53.
- [80] R. J. Bruls, H. T. Hintzen, R. Metselaar, C.-K. Loong, *J. Phys. Chem. Solids* **2000**, *61*, 1285–1293.
- [81] H. Hillebrecht, J. Churda, L. Schröder, H. G. von Schnering, *Z. Kristallogr. Suppl.* **1993**, *6*, 80.
- [82] J. Grins, Z. Shen, S. Esmaeilzadeh, *Silic. Ind.* **2004**, *69*, 9–13.
- [83] J. G. Thompson, R. L. Withers, S. R. Palethorpe, A. Melnichenko, *J. Solid State Chem.* **1998**, *141*, 29–49.
- [84] S. R. Römer, P. Kroll, W. Schnick, *J. Phys.: Condens. Matter* **2009**, *21*, 275407.
- [85] M. Zeuner, S. Pagano, S. Hug, P. Pust, S. Schmiechen, C. Scheu, W. Schnick, *Eur. J. Inorg. Chem.* **2010**, 4945–4951.
- [86] M. O’Keeffe, *Acta Crystallogr. Sect. A* **1992**, *48*, 670–673.
- [87] M. Marezio, J. P. Remeika, P. D. Dernier, *Acta Crystallogr. Sect. B* **1969**, *25*, 965–970.
- [88] N. L. Ross, R. J. Angel, *J. Solid State Chem.* **1991**, *90*, 27–30.
- [89] R. Mueller-Mach, G. O. Mueller, M. R. Krames, O. B. Shchekin, P. J. Schmidt, H. Bechtel, C.-H. Chen, O. Steigelmann, *Phys. Status Solidi RRL* **2009**, *3*, 215–217.
- [90] T. Schlieper, W. Milius, W. Schnick, Z. Anorg. Allg. Chem. **1995**, *621*, 1380–1384.
- [91] H. Huppertz, W. Schnick, *Acta Crystallogr. Sect. C* **1997**, *53*, 1751–1753.
- [92] S. R. Römer, C. Braun, O. Oeckler, P. J. Schmidt, P. Kroll, W. Schnick, *Chem. Eur. J.* **2008**, *14*, 7892–7902.
- [93] R. Mueller-Mach, G. Mueller, M. R. Krames, H. A. Höppe, F. Stadler, W. Schnick, T. Juestel, P. Schmidt, *Phys. Status Solidi A* **2005**, *202*, 1727–1732.
- [94] R.-J. Xie, N. Hirosaki, *Sci. Technol. Adv. Mater.* **2007**, *8*, 588–600.
- [95] Z. Inoue, M. Mitomo, N. Ii, *J. Mater. Sci.* **1980**, *15*, 2915–2920.
- [96] M. Woike, W. Jeitschko, *Inorg. Chem.* **1995**, *34*, 5105–5108.
- [97] J. Gaudé, J. Lang, D. Louer, *Rev. Chim. Miner.* **1983**, *20*, 523–527.
- [98] T. Schlieper, W. Schnick, Z. Anorg. Allg. Chem. **1995**, *621*, 1535–1538.
- [99] T. Schlieper, W. Schnick, *Z. Kristallogr.* **1996**, *211*, 254.
- [100] H. Huppertz, W. Schnick, Z. Anorg. Allg. Chem. **1998**, *624*, 371–374.
- [101] F. Stadler, O. Oeckler, W. Schnick, Z. Anorg. Allg. Chem. **2006**, *632*, 54–58.
- [102] H. Huppertz, W. Schnick, *Chem. Eur. J.* **1997**, *3*, 249–252.
- [103] G. Pilet, H. A. Höppe, W. Schnick, S. Esmaeilzadeh, *Solid State Sci.* **2005**, *7*, 391–396.
- [104] H. Huppertz, W. Schnick, *Angew. Chem.* **1996**, *108*, 2115–2116; *Angew. Chem. Int. Ed. Engl.* **1996**, *35*, 1983–1984.
- [105] H. Huppertz, W. Schnick, Z. Anorg. Allg. Chem. **1997**, *623*, 212–217.
- [106] Y. Q. Li, C. M. Fang, G. deWith, H. T. Hintzen, *J. Solid State Chem.* **2004**, *177*, 4687–4694.
- [107] A. Lieb, J. A. Kechele, R. Kraut, W. Schnick, Z. Anorg. Allg. Chem. **2007**, *633*, 166–171.
- [108] H.-C. Zhang, T. Horikawa, K.-I. Machida, *J. Electrochem. Soc.* **2006**, *153*, H151–H154.
- [109] H. A. Höppe, G. Kotzyba, R. Pöttgen, W. Schnick, *J. Mater. Chem.* **2001**, *11*, 3300–3306.
- [110] A. Friedrich, K. Knorr, B. Winkler, A. Lieb, H. A. Höppe, W. Schnick, V. Milman, M. Hanfland, *J. Phys. Chem. Solids* **2009**, *70*, 97–106.
- [111] F. Stadler, O. Oeckler, J. Senker, H. A. Höppe, P. Kroll, W. Schnick, *Angew. Chem.* **2005**, *117*, 573–576; *Angew. Chem. Int. Ed.* **2005**, *44*, 567–570.
- [112] F. Stadler, W. Schnick, Z. Anorg. Allg. Chem. **2007**, *633*, 589–592.
- [113] Z. Shen, J. Grins, S. Esmaeilzadeh, H. Ehrenberg, *J. Mater. Chem.* **1999**, *9*, 1019–1022.
- [114] F. Ottinger, *Doctoral Thesis*, ETH Zürich, 2004.
- [115] D. P. Thompson, *Mater. Sci. Forum* **1989**, *47*, 21–42.

- [116] C. Hecht, F. Stadler, P. J. Schmidt, J. Schmedt auf der Günne, V. Baumann, W. Schnick, *Chem. Mater.* **2009**, *21*, 1595–1601.
- [117] J. A. Kechele, C. Hecht, O. Oeckler, J. Schmedt auf der Günne, P. J. Schmidt, W. Schnick, *Chem. Mater.* **2009**, *21*, 1288–1295.
- [118] S. J. Clarke, F. J. DiSalvo, *Inorg. Chem.* **1997**, *36*, 1143–1148.
- [119] F. Ottlinger, E. Cuervo-Reyes, R. Nesper, *Z. Anorg. Allg. Chem.* **2010**, *636*, 1085–1089.
- [120] F. Ottlinger, I. Kroslakova, K. Hametner, E. Reusser, R. Nesper, D. Günther, *Anal. Bioanal. Chem.* **2005**, *383*, 489–499.
- [121] G. Pilet, J. Grins, M. Eden, S. Esmaeilzadeh, *Eur. J. Inorg. Chem.* **2006**, *3627*–3633.
- [122] V. Ischenko, L. Kienle, M. Jansen, *J. Mater. Sci.* **2002**, *37*, 5305–5317.
- [123] J. Grins, S. Esmaeilzadeh, Z. Shen, *J. Am. Ceram. Soc.* **2003**, *86*, 727–730.
- [124] K. H. Jack, *J. Mater. Sci.* **1976**, *11*, 1135–1158.
- [125] R. Lauterbach, W. Schnick, *Z. Anorg. Allg. Chem.* **2000**, *626*, 56–61.
- [126] J. W. H. van Krevel, H. T. Hintzen, R. Metselaar, *Mater. Res. Bull.* **2000**, *35*, 747–754.
- [127] F. Stadler, R. Kraut, O. Oeckler, S. Schmid, W. Schnick, *Z. Anorg. Allg. Chem.* **2005**, *631*, 1773–1778.
- [128] R. Lauterbach, W. Schnick, *Z. Anorg. Allg. Chem.* **1998**, *624*, 1154–1158.
- [129] W. Schnick, *Int. J. Inorg. Mater.* **2001**, *3*, 1267–1272.
- [130] R. Lauterbach, E. Irran, P. F. Henry, M. T. Weller, W. Schnick, *J. Mater. Chem.* **2000**, *10*, 1357–1364.
- [131] R. Lauterbach, W. Schnick, *Solid State Sci.* **2000**, *2*, 463–472.
- [132] O. Oeckler, J. A. Kechele, H. Koss, P. J. Schmidt, W. Schnick, *Chem. Eur. J.* **2009**, *15*, 5311–5319.
- [133] J. A. Kechele, O. Oeckler, P. J. Schmidt, W. Schnick, *Eur. J. Inorg. Chem.* **2009**, *3326*–3332.
- [134] D. Peters, E. F. Paulus, H. Jacobs, *Z. Anorg. Allg. Chem.* **1990**, *584*, 129–137.
- [135] S. I. Ali, *Z. Anorg. Allg. Chem.* **1970**, *379*, 68–71.
- [136] M. Orth, R. D. Hoffmann, R. Pöttgen, W. Schnick, *Chem. Eur. J.* **2001**, *7*, 2791–2797.
- [137] G. O. Brunner, W. M. Meier, *Nature* **1989**, *337*, 146–147.
- [138] R. D. Shannon, *Acta Crystallogr. Sect. A: Cryst. Found. Crystallogr.* **1976**, *32*, 751–767.
- [139] A. J. D. Barnes, T. J. Prior, M. G. Francesconi, *Chem. Commun.* **2007**, 4638–4640.
- [140] S. Correll, N. Stock, O. Oeckler, W. Schnick, *Angew. Chem.* **2003**, *115*, 3674–3677; *Angew. Chem. Int. Ed.* **2003**, *42*, 3549–3552.
- [141] S. Correll, N. Stock, O. Oeckler, J. Senker, T. Nilges, W. Schnick, *Z. Anorg. Allg. Chem.* **2004**, *630*, 2205–2217.
- [142] H. Huppertz, W. Schnick, *Angew. Chem.* **1997**, *109*, 2765–2767; *Angew. Chem. Int. Ed. Engl.* **1997**, *36*, 2651–2652.
- [143] C. Schmolke, O. Oeckler, D. Bichler, D. Johrendt, W. Schnick, *Chem. Eur. J.* **2009**, *15*, 9215–9222.
- [144] F. Karau, W. Schnick, *Angew. Chem.* **2006**, *118*, 4617–4620; *Angew. Chem. Int. Ed.* **2006**, *45*, 4505–4508.
- [145] R. Hoppe, *Angew. Chem.* **1966**, *78*, 52–63; *Angew. Chem. Int. Ed. Engl.* **1966**, *5*, 95–106.
- [146] R. Hoppe, *Angew. Chem.* **1970**, *82*, 7–16; *Angew. Chem. Int. Ed. Engl.* **1970**, *9*, 25–34.
- [147] R. Hübenthal, “MAPLE, Programm zur Berechnung des Madelunganteils der Gitterenergie”, Version 4, Universität Gießen **1993**.
- [148] H. A. Höpke, *Doctoral Thesis*, University of Munich (LMU), **2001**.
- [149] K. Köllisch, *Doctoral Thesis*, University of Munich (LMU), **2001**.
- [150] R. Lauterbach, *Doctoral Thesis*, University of Bayreuth, **1999**.
- [151] D. R. Clarke, *J. Am. Ceram. Soc.* **1987**, *70*, 15–22.
- [152] N. Shibata, S. J. Pennycook, T. R. Gosnell, G. S. Painter, W. A. Shelton, P. F. Becher, *Nature* **2004**, *428*, 730–733.
- [153] A. Ziegler, C. Kisielowski, M. J. Hoffmann, R. O. Ritchie, *J. Am. Ceram. Soc.* **2003**, *86*, 1777–1785.
- [154] M. J. Hoffmann, in *Tailoring of Mechanical Properties of Si<sub>3</sub>N<sub>4</sub> Ceramics*, *NATO ASI Series E, Applied Sciences*, Vol. 276, (Eds.: M. J. Hoffmann, G. Petzow), Kluwer, Dordrecht, **1994**.
- [155] L.-O. Nordberg, Z. Shen, M. Nygren, T. Ekström, *J. Eur. Ceram. Soc.* **1997**, *17*, 575–580.
- [156] S.-L. Hwang, H.-T. Lin, P. F. Becher, *J. Mater. Sci.* **1995**, *30*, 6023–6027.
- [157] I. J. McColm, *Ceramic Hardness*, Plenum, New York, London, **1990**.
- [158] G. A. Slack, *J. Phys. Chem. Solids* **1973**, *34*, 321–335.
- [159] M. P. Borom, G. A. Slack, J. W. Szymaszek, *Am. Ceram. Soc. Bull.* **1972**, *51*, 852–856.
- [160] G. A. Slack, R. A. Tanzilli, R. O. Pohl, J. W. Vandersande, *J. Phys. Chem. Solids* **1987**, *48*, 641–647.
- [161] R. J. Bruls, *Doctoral Thesis*, Eindhoven University of Technology, **2000**.
- [162] M. Kitayama, K. Hirao, Watari K., M. Toriyama, S. Kanzaki, *J. Am. Ceram. Soc.* **2001**, *84*, 353–358.
- [163] R. J. Bruls, H. T. Hintzen, R. Metselaar, *J. Eur. Ceram. Soc.* **2005**, *25*, 767–779.
- [164] R. J. Bruls, A. A. Kudyba-Jansen, P. Gerharts, H. T. Hintzen, *J. Mater. Sci. Mater. Electron.* **2002**, *13*, 63–75.
- [165] H. T. Hintzen, R. J. Bruls, A. C. A. Delsing, K. Itatani, S. Tanaka, G. de With, R. Metselaar, *Key Eng. Mater.* **2002**, *206–213*, 973–976.
- [166] H. Yamane, S. Kikkawa, M. Koizumi, *J. Power Sources* **1987**, *20*, 311–315.
- [167] D. R. MacFarlane, J. Huang, M. Forsyth, *Nature* **1999**, *402*, 792–794.
- [168] M. S. Bhamra, D. J. Fray, *J. Mater. Sci.* **1995**, *30*, 5381–5388.
- [169] S. R. Marder, G. D. Stucky, J. E. Sohn, *Materials for Nonlinear Optics: Chemical Perspectives*, ACS Symp. Ser. **1991**, 455.
- [170] D. S. Chemla, J. Zyss, *Nonlinear Optical Properties of Organic Molecules and Crystals*, Vols. 1, 2, Academic Press, New York, **1987**.
- [171] H. Lutz, S. Joosten, J. Hoffmann, P. Lehmeier, A. Seilmeier, H. A. Höpke, W. Schnick, *J. Phys. Chem. Solids* **2004**, *65*, 1285–1290.
- [172] S. K. Kurtz, T. T. Perry, *J. Appl. Phys.* **1968**, *39*, 3798–3813.
- [173] M. Kiguchi, M. Kato, N. Kumegawa, Y. Taniguchi, *J. Appl. Phys.* **1994**, *75*, 4332–4339.
- [174] R. Kremer, A. Boudrioua, J. C. Loulergue, A. Iltis, *J. Opt. Soc. Am. B* **1999**, *16*, 83–89.
- [175] H. Huppertz, *Doctoral thesis*, University of Bayreuth, **1997**.
- [176] H. A. Höpke, H. Lutz, P. Morys, W. Schnick, A. Seilmeier, *J. Phys. Chem. Solids* **2000**, *61*, 2001–2006.
- [177] S. Nakamura, M. Senoh, T. Mukai, *Appl. Phys. Lett.* **1993**, *62*, 2390–2392.
- [178] J. K. Park, K. J. Choi, J. H. Yeon, S. J. Lee, C. H. Kim, *Appl. Phys. Lett.* **2006**, *88*, 043511.
- [179] J. K. Park, C. H. Kim, S. H. Park, H. D. Park, S. Y. Choi, *Appl. Phys. Lett.* **2004**, *84*, 1647–1649.
- [180] D. Jia, D. N. Hunter, *J. Appl. Phys.* **2006**, *100*, 113125.
- [181] Y. R. Do, K. Y. Ko, S. H. Na, Y. D. Huh, *J. Electrochem. Soc.* **2006**, *153*, H142–H146.
- [182] C. Liu, J. Heo, *Mater. Lett.* **2007**, *61*, 3751–3754.
- [183] G. Lakshminarayana, H. Yang, J. Qiu, *J. Solid State Chem.* **2009**, *182*, 669–676.
- [184] K. Uheda, N. Hirosaki, Y. Yamamoto, A. Naito, T. Nakajima, H. Yamamoto, *Electrochim. Solid-State Lett.* **2006**, *9*, H22–H25.
- [185] P. Dorenbos, *Phys. Rev. B* **2000**, *62*, 15640–15649.
- [186] P. Dorenbos, *Phys. Rev. B* **2001**, *64*, 125117.

- [187] P. Dorenbos, *Phys. Rev. B* **2002**, *65*, 235110.
- [188] H. A. Höppe, *Angew. Chem.* **2009**, *121*, 3626–3636; *Angew. Chem. Int. Ed.* **2009**, *48*, 3572–3582.
- [189] A. A. Setlur, *Electrochem. Soc. Interface* **2009**, *18*, 32–36.
- [190] X.-H. He, N. Lian, J.-H. Sun, M.-Y. Guan, *J. Mater. Sci.* **2009**, *44*, 4763–4775.
- [191] J. W. H. van Krevel, H. T. Hintzen, R. Metselaar, A. Meijerink, *J. Alloys Compd.* **1998**, *268*, 272–277.
- [192] J. W. H. van Krevel, *Ph. D. Thesis*, Eindhoven University of Technology, **2000**.
- [193] Y. Q. Li, J. E. J. van Steen, J. W. H. van Krevel, G. Botty, A. C. A. Delsing, F. J. DiSalvo, G. de With, H. T. Hintzen, *J. Alloys Compd.* **2006**, *417*, 273–279.
- [194] F. Stadler, *Doctoral Thesis*, University of Munich (LMU), **2006**.
- [195] Y. Q. Li, G. de With, H. T. Hintzen, *J. Solid State Chem.* **2008**, *181*, 515–524.
- [196] O. B. Shchekin, J. E. Epler, T. A. Trottier, T. Margalith, D. A. Steigerwald, M. O. Holcomb, P. S. Martin, M. R. Krames, *Appl. Phys. Lett.* **2006**, *89*, 071109.
- [197] Y. Q. Li, A. C. A. Delsing, G. De With, H. T. Hintzen, *Chem. Mater.* **2005**, *17*, 3242–3248.
- [198] V. Bachmann, T. Juestel, A. Meijerink, C. Ronda, P. J. Schmidt, *J. Lumin.* **2006**, *121*, 441–449.
- [199] R.-S. Liu, Y.-H. Liu, N. C. Bagkar, S.-F. Hu, *Appl. Phys. Lett.* **2007**, *91*, 061119.
- [200] H. Watanabe, H. Yamane, N. Kijima, *J. Solid State Chem.* **2008**, *181*, 1848–1852.
- [201] H. Watanabe, M. Imai, N. Kijima, *J. Am. Ceram. Soc.* **2009**, *92*, 641–648.
- [202] R.-J. Xie, N. Hirosaki, M. Mitomo, Y. Yamamoto, T. Suehiro, K. Sakuma, *J. Phys. Chem. B* **2004**, *108*, 12027–12031.
- [203] H.-L. Li, N. Hirosaki, R.-J. Xie, T. Suehiro, M. Mitomo, *Sci. Technol. Adv. Mater.* **2007**, *8*, 601–606.
- [204] J. W. H. van Krevel, J. W. T. van Rutten, H. Mandal, H. T. Hintzen, R. Metselaar, *J. Solid State Chem.* **2002**, *165*, 19–24.
- [205] R.-J. Xie, N. Hirosaki, K. Sakuma, Y. Yamamoto, M. Mitomo, *Appl. Phys. Lett.* **2004**, *84*, 5404–5406.
- [206] R.-J. Xie, N. Hirosaki, M. Mitomo, K. Sakuma, N. Kimura, *Appl. Phys. Lett.* **2006**, *89*, 241103.
- [207] N. Hirosaki, R.-J. Xie, K. Kimoto, T. Sekiguchi, Y. Yamamoto, T. Suehiro, M. Mitomo, *Appl. Phys. Lett.* **2005**, *86*, 211905.
- [208] R.-J. Xie, N. Hirosaki, H.-L. Li, Y. Q. Li, M. Mitomo, *J. Electrochem. Soc.* **2007**, *154*, J314–J319.
- [209] M. Mikami, S. Shimooka, K. Uheda, H. Imura, N. Kijima, *Key Eng. Mater.* **2009**, *403*, 11–14.
- [210] C. M. Fang, H. T. Hintzen, G. de With, *J. Alloys Compd.* **2002**, *336*, 1–4.
- [211] C. M. Fang, H. T. Hintzen, R. A. de Groot, G. de With, *J. Alloys Compd.* **2001**, *322*, L1–L4.
- [212] C. M. Fang, H. T. Hintzen, G. de With, G. A. de Groot, *J. Phys.: Condens. Matter* **2001**, *13*, 67–76.